OPTICAL PROPERTIES OF NOVEL PHOTOSENSITIZERS FOR PHOTODYNAMIC THERAPY

by

Busenur Aslanoğlu

B.S., Integrated B.S.&M.S. Program in Teaching Chemistry, Bogaziçi University, 2019

Submitted to the Institute for Graduate Studies in
Science and Engineering in partial fulfillment of
the requirements for the degree of
Master of Science

Graduate Program in Chemistry
Boğaziçi University
2022

ACKNOWLEDGEMENTS

It has been five and a half years when I first took a step into the CCBG lab. It's been a journey that I couldn't even imagine. I'd like firstly to thank my supervisor Prof.Dr. Şaron Çatak for holding my hand at the very beginning and supporting me through all these years to become who I am right now.

I also would like to express my gratitude to Prof. Antonio Monari for all his support at every step of the way.

I would like to thank the member of my committee, Assoc. Prof. Başak Kayıtmazer for their valuable advice and comments. Also, I am grateful for the very pleasant and peaceful environment during my defense seminar.

I would like to thank TUBITAK by supporting this research via TUBITAK 1001 (120Z659) project. GPU resources were allocated by the Université de Lorraine as well as TUBITAK ULAKBIM High Performance and Grid Computing Center (TRUBA resources). All the figures in this thesis are reproduced from Ref. A.1 with permission from the Royal Society of Chemistry.

Gamze Tanriver, I feel lucky to have you as my mentor/friend from the very beginning, I will never forget the days and nights spent in the lab together. Beyza Horoz, you are my friend who is special and kind, who is always there for me, who is always a great support, I couldn't imagine days spent without you through all these years in Hisarüstü and, missing them already, but we're always "cool, cool, coool". Öyküm Avcı, hocam, I know you are somewhere in Europe only one facetime away, I am so grateful for all the memories we had and excited for the ones to come! and I'd like to make this phrase eternal "puis-je prendre une cigarette s'il vous plaît?". Oğuzhan Kucur, which country is awaiting us to travel? and now I am ready to say yes to the question "vous avez perdu?", I am so lucky to have you as my travel buddy!

Başak Koca, how can I forget all the help and guidance you provided? The best days are yet to come, get up, stand up and don't give up the fight! Thank you for always being there for me and I will be there for youu! Lastly, I would like to thank all the current and former CCBG members, you are the ones who make this place peaceful, joyful, and wonderful!

Can, any place on Earth or even Mars seems one ticket away with you, but let's figure it out on the way, comrade. In the very end, every single question has one single answer, right? 'Chicken chicken chicken'.

Lastly, I would like to express my deepest, heart-felted thanks to my family, for their unconditional love and support. If I had given a chance to come to this world again, I would choose you over and over again. It has been hard but it has been bearable thanks to you! I am the luckiest person on earth because of you, and I would like to dedicate my thesis to you. Love you, always.

ABSTRACT

OPTICAL PROPERTIES OF NOVEL PHOTOSENSITIZERS FOR PHOTODYNAMIC THERAPY

Computational chemistry plays an important role in interpreting various phenomena regarding properties of complex molecular and biological systems via several computational approaches. In this thesis, the full characterization of the photophysical properties of the temoporfin chromophore(mTHPC) and newly designed metal coordinated photosensitizer candidate (Zn-Ar) will be investigated in the light of molecular modeling and simulation techniques presently used in photodynamic therapy. Notably, the photosensitizers follows different photophysical pathways which lead to intersystem-crossing and thus, the triplet state population occurs. This is essential for producing the singlet oxygen, which leads to cell death.

In this thesis, molecular dynamics (MD) and quantum mechanics simulations, we employed to shed light on the formation of stable interactions between the temoporfin and the membrane; particularly, the penetration of temoporfin into its hydrophobic center. These processes will allow us to determine the specific interactions between temoporfin and the lipid oxidizable double bond pointing towards the production of singlet oxygen.

In addition to temoporfin, a novel photosensitizer candidate was investigated with the same protocol. This novel photosensitizer candidate will expose the effects of the metal coordinated chromophores and their photodynamic therapy abilities.

ÖZET

FOTODİNAMİK TERAPİ İÇİN ÖZGÜN FOTO DUYARLAŞTIRICILARIN OPTİK ÖZELLİKLERİ

Hesapsal kimya, çeşitli moleküler ve biyolojik sistemlerin özelliklerine ilişkin fenomenleri kuantum mekanik ve moleküler mekanik gibi farklı yaklaşımları kullanarak yorumlamada önemli bir role sahiptir. Bu tezde, temoporfin kromoforunun (mTHPC) ve yeni tasarlanmış metal koordineli ışığa duyarlılaştırıcı adayının (Zn-Ar) fotofiziksel özelliklerinin tam karakterizasyonu, günümüzde fotodinamik terapide kullanılan moleküler modelleme ve simülasyon teknikleri ışığında araştırılacaktır. Özellikle, ışığa duyarlılaştırıcılar, sistemler arası geçişe yol açan farklı fotofiziksel yolları takip etmektedir ve böylece triplet uyarılmış halde bir popülasyon oluşturabilirler. Bu durum, hücre ölümüne yol açan singlet oksijenin üretilmesi için gereklidir.

Bu tezde, moleküler dinamik (MD) ve kuantum mekanik simülasyonlarıyla birlikte, temoporfinin membran ile hidrofilik ve hidrofobik etkileşimlerinin sonuçları verilecektir. Bu süreçler, temoporfinin singlet oksijen üretimine işaret edip, ışığa duyarlılaşmayı destekleyen lipid ile oksitlenebilir çift bağ arasındaki etkileşimi belirlememize izin verecektir.

Temoporfine ek olarak, bir diğer ışığa duyarlılaştırıcı adayı da aynı protokolle araştırılmıştır. Bu yeni ışığa duyarlılaştırıcı adayının araştırılmasının nedeni, metal koordineli kromoforların etkilerini ve bunların fotodinamik terapi için yeterliliklerini ortaya çıkarmaktır.

TABLE OF CONTENTS

ACKNOWLEDGEMENTS iii
ABSTRACT v
ÖZET vi
LIST OF FIGURES ix
LIST OF TABLES xiii
LIST OF SYMBOLS xiv
LIST OF ACRONYMS/ABBREVIATIONS xv
1. INTRODUCTION 1
1.0.1. Background for Photodynamic Therapy 1
1.0.2. Mechanism of Photodynamic Therapy 2
1.0.3. Requirements for Photodynamic Therapy 3
2. METHODOLOGY 7
2.1. Density Functional Theory 7
2.2. Time Dependent Density Functional Theory 8
2.3. Wigner Distribution Function 9
2.4. Computational Choices 10
2.4.1. Functional 10
2.4.2. Basis Set 10
2.4.3. Continuum Solvation Model 11
3. AIM OF THE STUDY 13
4. RESULT AND DISCUSSION 14
4.1. Preparation of the Systems 14
4.1.1. Quantum Mechanics Molecular Dynamics 14
4.1.2. Classical Molecular Dynamics and Force Field Parametrization . 14
4.1.3. Electronic Structure Calculations 15
4.2. Investigation of Temoporfin (mTHPC) 19
4.2.1. Dihedral Angle Distribution Analysis of Temoporfin (mTHPC) . 19
4.2.1.1. mTHPC in vacuum 20

4.2.1.2. mTHPC in water 23
4.2.1.3. mTHPC:TM-β-CD complex 24
4.2.1.4. mTHPC:POPC 26
4.2.2. Absorption Spectra Analysis of Temoporfin (mTHPC) 27
4.2.2.1. mTHPC in vacuum 28
4.2.2.2. mTHPC in water 29
4.2.2.3. mTHPC in TM-β-CD 30
4.2.2.4. mTHPC:POPC 31
4.2.3. Specific Interactions of mTHPC:POPC 33
4.3. Investigation of Metal Coordinated Chlorin (Zn-Ar) 36
4.3.1. Dihedral Angle Analysis of Metal Coordinated Chlorin (Zn-Ar) 36
4.3.1.1. Zn-Ar in Vacuum 36
4.3.1.2. Zn-Ar in water 37
4.3.2. Absorption Spectra Analysis of Metal Coordinated Chlorin (Zn-Ar) 38
4.3.2.1. Zn-Ar in vacuum 38
4.3.2.2. Zn-Ar in water 39
4.4. Comparison of mTHPC with Zn-Ar 39
4.4.1. Absorption Spectra Comparison of mTHPC and Zn-Ar 40
5. CONCLUSION 42
5.0.1. Future Remarks 43
REFERENCES 44
APPENDIX A: ARTICLES 59
A.1. Optical Properties of Photodynamic Therapy Drugs in Different Environments: The Paradigmatic Case of Temoporfin 59
APPENDIX B: Root-Mean-Square-Deviation Values of mTHPC from different environments 68

LIST OF FIGURES

Figure 1.1. Jablonski Diagram to display cell death mechanism. 2

Figure 1.2. 3-D structure of Temoporfin (mTHPC) photosensitizer 4

Figure 1.3. 3-D structure of newly designed zinc coordinated chlorin (Zn-Ar) photosensitizer candidate. 5

Figure 4.1. Computational details of mTHPC for each environment. Simulation 1 is for Quantum Mechanics, Simulation 2 is for oldFF classical Molecular Dynamic Simulations and Simulation 3 is for the newFF classical Molecular Dynamics Simulations. 18

Figure 4.2. Encapsulated temoporfin in TM-β-CD complex with *intra* (in orange) and *inter* (in yellow). 20

Figure 4.3. Rotational free energy (M062X/6-31+G(d)) profile for a dihedral scan. The geometry of the molecule in the three points a, b and c is displayed in the bottom panel. 21

Figure 4.4. Distribution of the *inter* (a) oldFF (c) newFF and *inter* (b) oldFF (d) newFF dihedrals of mTHPC in vacuum extracted from classical MD. 22

Figure 4.5. Distribution of the inter (left) and intra (right) dihedrals of mTHPC in vacuum during QM MD calculations. 23

Figure 4.6. Dihedral distribution of the inter (left) and intra (right) dihedrals in mTHPC in water during Classical MD (top) QM/MM MD simulations (bottom). 24

Figure 4.7. Distribution of the inter (a) newFF (c) QM/MM MD and intra (b) newFF (d) QM/MM MD dihedrals of mTHPC in water extracted from Classical MD. 25

Figure 4.8. mTHPC contacts with double bond C-C of POPC lipid bilayer where the singlet oxygen generation occurs. 26

Figure 4.9. Distribution of the inter (left) and intra (right) dihedrals for mTHPC in POPC lipid during Classical MD simulation. 27

Figure 4.10. Benchmark to determine the functional and the basis set. 28

Figure 4.11. Absorption spectra of mTHPC in vacuum calculated by classical MD and QM MD. 29

Figure 4.12. Absorption spectra of mTHPC in water calculated by classical MD and QM/MM MD. 30

Figure 4.13. Absorption spectra of mTHPC complex with TM-β-CD in water calculated by classical MD and QM/MM MD. 31

Figure 4.14. mTHPC absorption spectra in POPC lipid bilayer through 100 ns MD simulation. 32

Figure 4.15. Hydrogen bonding between hydrogen of the temoporfin phenol and the phosphate oxygen at the PC part of the POPC lipid. 33

Figure 4.16. Hydrogen bonding between hydrogen of the temoporfin phenol and the phosphate oxygen at the PC part of the POPC lipid. 34

Figure 4.17. Cation-π interaction between the temoporfin chlorine ring with the N atom at the PC side of the POPC lipid. 34

Figure 4.18. Cation-π interaction between the temoporfin chlorine ring with the N atom at the PC side of the POPC lipid. 35

Figure 4.19. Dihedral angle which is indicated with an orange color of the carbon atoms of the pyrroline ring around the chlorin core of Zn-Ar. . . 36

Figure 4.20. Dihedral angle distribution of atoms for phenyl ring positioned near pyrroline 37

Figure 4.21. Dihedral distribution of the selected atoms on phenyl ring of chlorin in water. 37

Figure 4.22. Absorption Spectrum of the Zn-Ar in gas. 38

Figure 4.23. Absorption Spectrum of the Zn-Ar in water. 39

Figure 4.24. Absorption Spectra of the Zn-Ar and mTHPC in vacuum. 40

Figure 4.25. Absorption Spectra of the mTHPC in water from Classical MD and QM/MM MD vs mTHPC in ethanol experimental result. 41

Figure A.1. Optical Properties of Photodynamic Therapy Drugs in Different Environments: The Paradigmatic Case of Temoporfin 59

Figure B.1. mTHPC in vacuum calculation from (a) QM/MD (b) oldFF (c) newFF 68

Figure B.2. mTHPC in water calculation from (a) QM/MD (b) oldFF (c) newFF 69

Figure B.3. mTHPC in TM-β-CD calculation from (a) newFF (b) QM/MD . . 69

Figure B.4. mTHPC in TM-β-CD calculation from (a) newFF (b) carbon atoms of mTHPC at inter position (c) carbon atoms of mTHPC at inter position 70

Figure B.5. mTHPC in POPC lipid bilayer from Classical MD calculation with newFF 70

LIST OF TABLES

4.1 Details of the Zn-Ar simulations 16

LIST OF SYMBOLS

E_{el}	Electronic Energy
$E_c[\rho]$	Correlation Energy
$E_x[\rho]$	Exchange Energy
$E_{XC}[\rho(r)]$	Exchange-Correlation Energy Functional
f	Oscillator Strength
G_{gs}^{HF}	Ground State Energy
H	Hamiltonian Operator
h_{KS}	Kohn-Sham Hamiltonian Operator
$P(r)$	Parr Function
q_A	Atomic Charge
$J[\rho(r)]$	Coulomb Energy
$T[\rho(r)]$	Kinetic Energy of Interacting Electrons
$T_{ni}[\rho(r)]$	Kinetic Energy of Non-Interacting Electrons
$V_{ext}(r)$	External Potential
$V_{ee}[\rho(r)]$	Electron-Electron Interactions
$V_{XC}[\rho(r)]$	Exchange-Correlation Potential
Z	Atomic Number
ε	Dielectric Constant
$\rho(r)$	Electron Density
ϕ_s	Quantitative Topological Descriptor
k^a	Local Stretching Force Constant
$\rho(r)$	Electron Density
H(r)	Energy Density
ψ_i	Kohn-Sham Orbitals
Ψ	Wavefunction

LIST OF ACRONYMS/ABBREVIATIONS

ACQ	Aggregation-Caused Quenching
atm	Atmosphere
B3LYP	Becke-3-Parameter Lee-Yang-Parr Functional
CHARMM-GUI	Chemistry at Harvard Macromolecular Mechanics Web-Based Graphical User Interface
DFT	Density Functional Theory
eV	Electron Volt
EWG	Electron Withdrawing Group
FDA	U.S. Food and Drug Administration
fs	Femtosecond
FWHL	Full Width at Half-Length
GAFF	General AMBER Force Field
GGA	Generalized Gradient Approximation
GTO	Gaussian Type Orbital
HF	Hartree-Fock Theory
HOMO	Highest Occupied Molecular Orbital
IEF-PCM	Integral Equation Formalism of Polarizable Continuum Model
IC	Internal Conversion
inter	Phenol Rings of Temoporfin which Stands between Two TM-β-CDs
intra	Phenol Rings of Temoporfin which are Encapsulated by Two TM-β-CD
ISC	Intersystem Crossing
IRC	Intrinsic Reaction Coordinate
K	Kelvin
LAC	Light-Assisted Chemotherapy
LDA	Local Density Approximation
LUMO	Lowest Unoccupied Molecular Orbital
M06-2X	Hybrid Meta Exchange-Correlation Functional

MD	Molecular Dynamics
MM	Molecular Mechanics
MP2	Moller–Plesset Perturbation Theory
mTHPC	(5,10,15,20-tetrakis(3-hydroxyphenyl)chlorin
newFF	New Force Field to Define Temoporfin
NCI	Non-Covalent Interactions
nm	Nanometer
NPT	Isothermal–Isobaric Ensemble
ns	Nanosecond
oldFF	Old Force Field to Define Temoporfin
PDT	Photodynamic Therapy
PBC	Periodic Boundary Conditions
PS	Photosensitizer
PES	Potential Energy Surface
PCM	Polarizable Continuum Model
PME	Particle-Mesh Ewald
POPC	1-Palmitoyl-2-oleoylphosphatidylcholine
QM	Quantum Mechanics
QM/MM	Quantum Mechanics Molecular/Molecular Mechanics
QM/MM MD	Quantum Mechanics/Molecular Mechanics Molecular Dynamics
$^1O_2$	Singlet Oxygen
STO	Slater Type Orbital
TD-DFT	Time-dependent density-functional theory
TIP3P	Transferable Intermolecular Potential with 3 Points Water Model
TM-β-CD	Trimethyl-Beta-Cyclodextrin
UV-vis	Ultraviolet–Visible Spectroscopy
VMD	Visual Molecular Dynamics
ωB97xD	Long-Range Corrected Hybrid Functional with Dispersion Correction

1. INTRODUCTION

This thesis focuses on employing computational methodologies to investigate the ability of two drug molecules on a non-invasive cancer treatment method, known as Photodynamic Therapy. Chapter 4.2 contains the results from the investigation of the drug molecule called temoporfin (mTHPC) which is an FDA approved drug with the brand name Foscan. Chapter 4.3 contains the results from the exploration of newly designed metal coordinated photosensitizer (Zn-Ar), and is efficiency for Photodynamic Therapy. Finally, the results from mTHPC and Zn-Ar are compared and findings are discussed thoroughly.

1.0.1. Background for Photodynamic Therapy

The exploitation of light as a therapeutic agent for the treatment of diverse and problematic diseases has gained large popularity in the last few decades, [1] paving the way to the definition of novel and less invasive, yet efficient, therapeutic strategies. This has most notably involved the treatment of bacterial and viral diseases, [2, 3] as well as more debilitating conditions such as some type of cancers [4–6]. However, the use of light for therapeutic purposes may be traced back to Ancient Greece, where exposure to sunlight, termed heliotherapy, was commonly used to treat a variety of conditions, including muscular weakness and skin diseases [6, 7]. The importance of such practices is also reflected in the fact that the god Apollon was associated with both medicine and the Sun.

Today the therapeutic use of light has evolved considerably, particularly owing to the milestone discovery and application of photodynamic therapy (PDT) [8, 9]. In this context, a drug that is inert in the dark is administered to a patient, either topically or systemically, and the region in which the lesion is localized is then irradiated, usually with visible or infrared light [10]. The absorption of light by the drug – the photosensitizer – triggers photophysical pathways leading to the disruption of biologi-

cal macromolecules (nucleic acids, proteins, or lipid membranes) and, consequently, to cell death, and ultimately to the eradication of the lesion [11].

1.0.2. Mechanism of Photodynamic Therapy

Although photophysical or photochemical pathways subsequent to light absorption may be diverse, two main families of events can be underlined: type I reactions involve either hydrogen abstraction or electron transfer from the excited photosensitizer (PS) to a substrate molecule to produce free radicals or radical ions [12]. Type II reactions transfer energy to molecular oxygen to produce singlet oxygen $^1O_2$ [13]. In particular, type II pathways usually proceed through intersystem crossing (ISC) populating the photosensitizer's triplet state manifold allowing the activation of the molecular oxygen from its triplet $^3O_2$ to singlet $^1O_2$ state [14]. Subsequently, the action of $^1O_2$ will induce the oxidative stress responsible for cell death [15]. PDT has proven efficient in the treatment of a variety of diseases, including psoriasis [16] as well as certain types of cancer, [17] such as esophageal [18] and cervical, [19] greatly limiting the side-effect of conventional therapy due to the spatial-selectivity of irradiation. [20, 21] These two pathways is explained with Jablonski diagram in Figure 1.1.

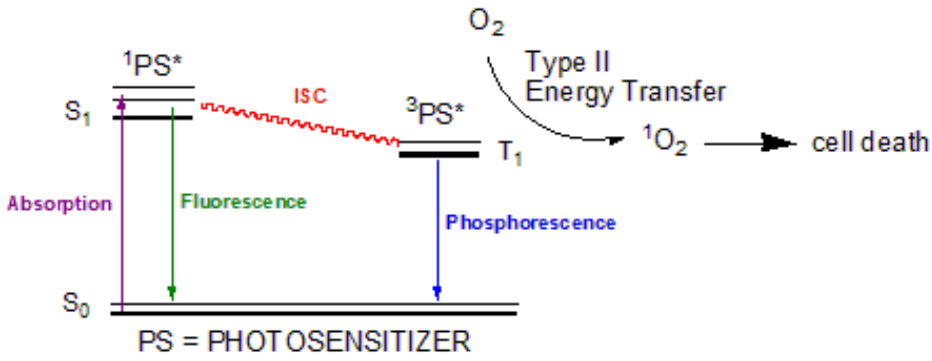

Figure 1.1. Jablonski Diagram to display cell death mechanism.

1.0.3. Requirements for Photodynamic Therapy

There are several requirements that should be met by PDT agents to increase their efficiency and guarantee their therapeutic effects [22]. These include: facile ISC, high quantum yield for the production of $^1O_2$ [23], absorption in the red or infrared portion of the electromagnetic spectrum to cover the therapeutic window for which penetration into tissues is maximal [24], as well as enhanced selectivity towards bacterial [25] or cancer cells [26]. However, the need for oxygen activation in PDT may present an obstacle for the treatment of hypoxic solid tumors [27]. Hence, the exploitation of different photochemical pathways, such as photodissociation, have been proposed under the general name of light-assisted chemotherapy (LAC) [27–30]. Although various agents have been proposed for PDT, nowadays, the quasi-totality of clinically approved agents are based on porphyrins [31], phthalocyanines [32], or chlorins [33–36]. These classes of molecules display red-shifted absorption, which may be further modulated by the inclusion of metal in the coordination sphere [31, 36, 37], relatively good ISC quantum yields as well as versatile and economic synthetic viability. One of the most efficient PDT drugs on the market nowadays, yet still plagued by aggregations [38], is the so-called temoporfin (5,10,15,20-tetrakis(3-hydroxyphenyl)chlorin – mTHPC. Marketed in the EU under the brand name Foscan [39], mTHPC is a synthetic tetrapyrrole, a partially hydrogenated porphyrin derivative, known as chlorin, Figure 1.2. Temoporfin is a second-generation photosensitizer, which has higher skin penetration, deeper light penetration, and lower biotoxicity, and moreover, it requires shorter treatment time as well as a lower light dosage to achieve the desired PDT response compared with other clinically approved photosensitizers, such as hematoporphyrin derivatives and photofirin [39]. Indeed, mTHPC possesses appropriate photophysical properties: excitation to the first excited singlet state by red light (630–680 nm) [40], and efficient ISC to a longer-lived excited triplet state, which has recently been rationalized by molecular modeling [41]. The latter triplet state may produce cytotoxic species by either a type I or type II reaction typical of photosensitizer agents used in photodynamic therapy [42].

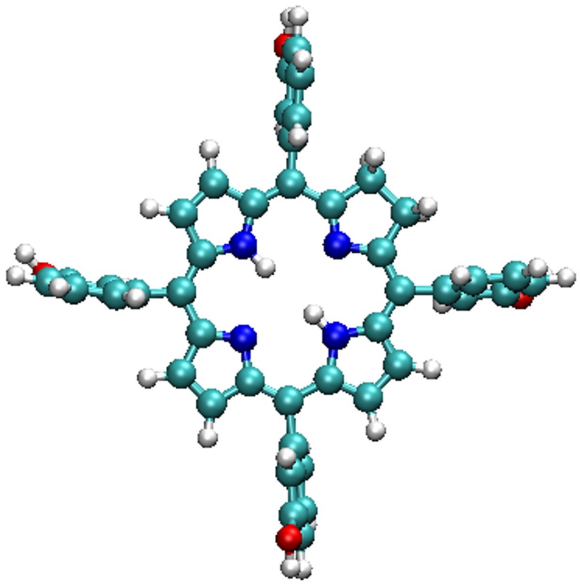

Figure 1.2. 3-D structure of Temoporfin (mTHPC) photosensitizer

A clear rationalization of the different aspects of PDT at the atomistic and electronic levels represents a challenge, since it requires multiscale modelling that is able to deal with both the treatment of excited states and the sampling of complex environments. In this respect, the development of PDT drug delivery systems represents a most paradigmatic case, since it requires the proper exploration of the conformational space of complex systems in complex environments, and at the same time, the need to provide a balanced description of physical and chemical phenomena taking place in both the ground and excited state manifolds [34]. The displacement of the absorption spectrum towards the red is pursued via different chemical strategies, including the use of organometallic complexes [43, 44]. For this purpose, the newly designed metal coordinated chlorin derivative as a photosensitizer candidate is also investigated in different environments and the results are compared accordingly. Zinc-metal core coordinated with the chlorin ring is abbreviated as Zn-Ar, Figure1.3. Metal addition to the photosensitizer is promising due to the greater coordination with the photosensitizer which results with greater ability to ISC [45].

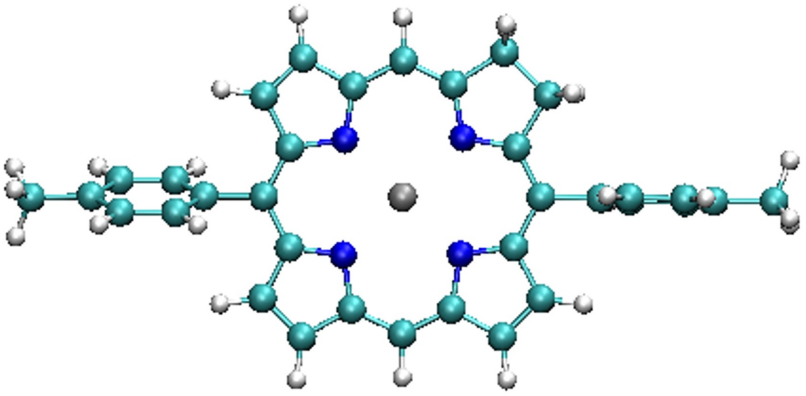

Figure 1.3. 3-D structure of newly designed zinc coordinated chlorin (Zn-Ar) photosensitizer candidate.

As mentioned, the most serious drawback of these two photosensitizers, and many other organic sensitizers, is their hydrophobic nature, which severely limits their transportation in the bloodstream and causes aggregation-caused quenching (ACQ) in biological environments [46], hence resulting in weak emissions and inadequate generation of reactive oxygen species (ROS) [47, 48]. To overcome the aggregation issue, specific drug delivery strategies are currently being pursued [43], in particular, the use of molecular hosts based on trimethyl-beta-cyclodextrin (TM-β-CD) has been proposed [49, 50]. The incorporation of mTHPC into TM-β-CD [51] and its release in model lipid membranes [52, 53] and cells [54, 55] have been experimentally assessed by monitoring its fluorescence quenching. Most notably, the encapsulation of mTHPC in trimethyl-β-cyclodextrin (TM-β-CD) also produces a strong enhancement of the fluorescence quantum yield that is almost totally quenched in solution, hence allowing for the possibility to efficiently follow drug delivery by optical spectroscopy. In particular, the complex systems involved in drug delivery and their interactions with biological structures requires the use of dynamic simulations using force field-based descriptions, also due to the key temporal spans that need to be covered. However, the sensitivity of excited state properties to even the slightest structural modifications also requires careful parameterization of the force fields [56–58]. In this study, we report the optical and photophysical properties of mTHPC employing molecular simulations in different

environments: (a) in vacuum, (b) in solution, (c) in solution encapsulated within TM-b-cyclodextrin (mTHPC:TM-β-CD complex), and (d) in interaction with a lipid bilayer mimicking a biological membrane. [59]. In parallel, Zn-Ar is investigated (a) in vacuum and (b) in water and the preliminary investigation results shows the effectiveness of metal coordination.

2. METHODOLOGY

2.1. Density Functional Theory

Density Functional Theory is established by Hohenberg and Kohn in order to unearth the ground state of a system interacting electrons. The theory is based on the Schrödinger's equation and consists of two theorems. First theorem explains the external potential $\mathbf{V}_{\text{ext}}(r)$ which is determined by a system containing electrons which means that by electron density ρ(r).

The electron density is represented as

$$\rho(r) : N \int \cdots \int |\Psi\left(r_1, r_2, \ldots r_n\right)|^2 dr_1 dr_2 \ldots dr_n. \tag{2.1}$$

.

Second theorem which is also called a Hohenberg-Kohn Variational theorem defines that minimum energy of a system depicts the true ground state electronic energy which is explained by the function of the electron density

$$E[\rho(r)] = \int V(r)\rho(r)dr + T[\rho(r)] + V_{ee}[\rho(r)]. \tag{2.2}$$

Kohn-Hohenberg succeeded to present the concept of non-interacting electrons through a reference system in 1965. The electronic energy equation becomes

$$E[\rho(r)] = \int V(r)\rho(r)d(r) + T_{ni}[\rho(r)] + J[\rho(r)] + E_{xc}[\rho(r)]. \tag{2.3}$$

$J[\rho(r)]$ indicates the coulomb energy meanwhile $E_{xc}[\rho(r)]$ defines the exchange-correlation energy functional and T_{ni} represents the kinetic energy.

Kohn-Sham equations are solved by Kohn-Sham orbitals

$$ {}_{i}^{KS}\chi_i = \varepsilon_i \chi_i. \tag{2.4} $$

and the Kohn-Sham Hamiltonian operator h_i^{KS} defines as:

$$ h_i^{KS} = -\frac{\nabla^2}{2} - \sum_{k}^{M} \frac{Z_k}{|r_i - r_k|} + \int \frac{\rho(r)}{r_{ij}} dr + V_{xc}. \tag{2.5} $$

V_{xc} represents the exchange correlation potential. If the exact exchange-correlation functional is known, Kohn-Sham orbitals can relinquish the exact density

$$ \rho(r) = \sum_{i=1}^{N} |\psi_i|^2 . \tag{2.6} $$

Since the exact form of exchange-correlation functional can not be known, approximate forms of functionals are developed.

2.2. Time Dependent Density Functional Theory

Time Dependent Functional Theory (TD-DFT) is the skeleton for the quantum mechanical approach for the calculations of excited state of the molecules.TD-DFT calculations are based on the Runge-Gross (RG) theorem which states that a given wavefunction associates with time-dependent density and time-dependent external potential. The Hamiltonian equation is

$$ \widehat{H} = \widehat{T}(\underline{r}) + \widehat{W}(\underline{r}) + \widehat{V}_{ext}(\underline{r}, t). \tag{2.7} $$

The sum of the kinetic energy of the electrons $\widehat{T}$, the Coulomb interactions between the electrons (electron-electron repulsion term) $\widehat{W}$, and time-dependent potential on the electrons $\widehat{V_{ext}}$. External potential has a crucial effect to define the electronic states of the molecule which depends on the external potential.

Wave function depends on the time constant and the square of wave function depicts the probability of locating an electron at a given time, which is demonstrated as

$$\rho(r,t) = N \int d^3r_2 \ldots d^3r_N \left|\Psi\left(r, r_2 \ldots r_N, t\right)\right|^2. \tag{2.8}$$

2.3. Wigner Distribution Function

The Wigner Distribution Function (Wigner quasi-probability distribution or Wigner-Ville distribution) is a quantum mechanical approach for relating wave function to probability distribution in phase space. Eugene Wigner first introduced it in 1932, and it has a wide range of applications, including amplitude and phase retrieval, signal processing, optical systems and devices, and phase space coupling coefficient computation. The Wigner distribution can be generated using either coordinate-space or momentum-space wave functions. The Wigner transform for a one-dimensional system can be stated as follows using the coordinate-space function:

$$W(x,p) = \frac{1}{2\pi} \int_{-\infty}^{\infty} \psi^* \left(x + \frac{s}{2}\right) \psi \left(x - \frac{s}{2}\right) e^{ips} ds. \tag{2.9}$$

where ψ denotes the wave function, p represents momentum, and x indicates location. The term $\psi^* \left(x + \frac{s}{2}\right)$ can be rewritten in the following way

$$\psi^* \left(x + \frac{s}{2}\right) = \left\langle \psi \mid x + \frac{s}{2} \right\rangle. \tag{2.10}$$

And the term $\psi \left(x - \frac{s}{2}\right)$ in Equation2.10 can be expressed as

$$\psi \left(x - \frac{s}{2}\right) = \left\langle x - \frac{s}{2} \mid \psi \right\rangle. \tag{2.11}$$

2.4. Computational Choices

2.4.1. Functional

One of the disadvantages of Density functional theory is the unknown exchange-correlation term E_{xc}. Different methodologies have been developed to overcome this shortfall, one of them is Local Density Approximation. LDA is originated on an assumption that electron density is same in each site of a system, therefore the system is assumed as homogeneous. This approach to the electron density as a uniform electron gas generates a gap which is filled by Generalized gradient approximation (GGA). GGA considers the electron density as a non-homogeneous system by proposing the exchange and correlation energies dependent on density gradient:

$$E_{xc}^{GGA}[n] = \int drn(r)\epsilon_{xc}(n(r), |\nabla n(r)|). \tag{2.12}$$

Alternative approaches include hybrid density functionals, which incorporate GGA with such a percentage of exact functionals. The most well-known hybrid density functional, B3LYP [35], is based on the GGA and LDA functionals:

$$E_{xc}^{BSLYP} = (1-a)E_x^{LSDA} + aE_x^{HF} + b\Delta E_x^B + (1-c)E_c^{LSDA} + cE_c^{LYP}. \tag{2.13}$$

B3LYP is insufficient in some circumstances, such as polarizability of longer chains and in TD-DFT calculations like excitations, and at that point ωB97X - D is employed [60]. This functional utilizes the version of Grimme's D2 dispersion model [61].

2.4.2. Basis Set

Basis sets can be investigated into two main categories; one of them is Slater-type orbitals (STOs) [62] developed by John C. Slater, which provides a solution for the Schrödinger equation of hydrogen like atoms, but STOs have high computational

cost due to the considerable amount of required integrals that needs to account. On the other hand, Gaussian-type orbitals (GTOs) [63] developed by S. Francis Boys, provide computational practicality due to their simpler formula.

Split valence basis sets were developed by John Pople to reduce computational cost [64]. The main principal is splitting valence orbitals from the core, so that core electrons can be treated with minimal basis set, since valence electrons can be treated more cautiously. This core electrons are minimally affected by the chemical environment compared to valence electrons. Some examples of split valence basis sets are 6-31+G, 3-21G, 6-311G*. The first number before the dash represents the number of Gaussian functions for core electrons meanwhile the numbers stated after the dash indicates the number of Gaussian functions for valence electrons

For a better approximation for the exact electronic energy, polarization and diffusion functions are introduced to the split valence basis sets. For heavy atoms, polarization function provide higher angular momentum. Polarization functions are represented in basis set with asterisk (*) or or (d) which means that the basis sets considers the p orbitals. For hydrogen-like atoms, double asterisk (**) or (d,p) is used. Diffusion functions are crucial for defining the atoms with high electron density. Diffuse functions are indicated in the basis set with "+" which means that only p orbitals are treated with diffuse function. Addition of one more "+" like "++" in the basis set denotes that s orbitals are considered as well.

2.4.3. Continuum Solvation Model

Specifying the environment around a molecular system to obtain more accurate results have a great importance in quantum chemical calculations. Effect of solvent can be considered explicitly or implicitly. Explicit solvation models recognize each single solvent molecule separately which creates a high computational cost. Implicit solvation models characterize their environment as a polarizable medium by a static dielectric

constant. Total solvation free energy is depicted as:

$$\Delta G_{\text{solvation}} = \Delta G_{\text{cavity}} + \Delta G_{\text{dispersion}} + \Delta G_{\text{electrostatic}} + \Delta G_{\text{repulsion}} .$$

ΔG_{cavity} defines the required free energy in order to build the cavity for solute; $\Delta G_{\text{dispersion}}$ represents the dispersion interactions between the solvent and the solute; $\Delta G_{\text{electrostatic}}$ indicates the electrostatic interaction between solvent and solute; and $\Delta G_{\text{repulsion}}$ is the exchange solute-solvent interactions.

Polarizable Continuum Model was introduced by Tomasi *et al.* [65] The model is developed as the cavity is defined by union spheres centering each atom, having radii identified by the van der Waals radii of the atoms multiplied by a constant factor.

3. AIM OF THE STUDY

This study focuses on two choromophore molecules [66]; one of which is an FDA-approved drug and the other is a newly designed metal coordinated molecule. Both are investigated for their efficiency for the photodynamic therapy.

Investigation is held primarily for the temoporfin (mTHPC) photosensitizer whose official brand name is Foscan. Secondarily, a derivative of the temoporfin molecule which is coordinated with a zinc atom is investigated. Optical and photophysical properties of both molecules are investigated thoroughly. Photodynamic therapy efficiencies are rationalized via investigation in complex environments.

4. RESULT AND DISCUSSION

This chapter contains three sections; the first part contains the results from the investigation of mTHPC; and the second part contains the results from the exploration of a newly designed metal coordinated photosensitizer (Zn-Ar) for Photodynamic Therapy. Finally, the results from both studies are compared and findings are discussed.

4.1. Preparation of the Systems

Temoporfin (mTHPC) molecule is investigated with quantum mechanical/molecular dynamics and classical molecular dynamic simulations in four different environments which are in vacuum, in water, in complex with TM-β-CD and in POPC lipid bilayer, 1-palmitolyl-2-oleyl-sn-glycero- 3-phosphocholine (POPC). Meanwhile Zn-Ar is investigated via classical molecular dynamic simulations in vacuum and in water.

4.1.1. Quantum Mechanics Molecular Dynamics

Quantum mechanics/molecular dynamic simulations are an hybrid method, which is performed on the ground state conformational space via Terachem [67] and AMBER/Terachem [68] interface. Photosensitizers are treated in the QM partition with B3LYP density functional theory and 6-31G basis set; meanwhile surrounding water and TM-β-CD are included in MM level with force field parametrization.

4.1.2. Classical Molecular Dynamics and Force Field Parametrization

NAMD program package is used for the calculation of classical MD simulations [69]. All simulations are conducted to integrate Newton's equations of motion in constant pressure and temperature ensemble (NPT) [70] at 1 atm and 300.0 K, meanwhile the time step selected is 2.0 fs. 100 ns production run is performed after equilibration and thermalization. Langevin thermostat [71] and Nosé-Hoover Langevin

barostat [72] controlled the temperature and pressure, respectively. In order to approximate the large system into the small unit cell, Periodic Boundary Conditions(PBC) is used and calculation of long-range electrostatics contributions is conducted via using Particle Mesh Ewald (PME) [73] with a 9 Å cutoff distance.

POPC unit is prepared by using Lipid14 General Amber Force Field [74] meanwhile CHARMM-GUI interface is used to set up lipid bilayer. Each membrane leaflet consists of 100 POPC units and full hydration of bilayer is provided by 37 551 water molecules and is neutralized by 104 K+ and Cl- ions. The total box size is 81.0 x 81.0 x 138.0 $\mathring{A}^3$. Using the lipid membrane model is an oversimplified version of a biological environment, due to the fact that structural properties of the membrane may also be affected by the presence of other fatty acids or cholesterol. Nevertheless, the use of a single lipid, greatly reduces the degrees of freedom, while still providing a realistic amphiphilic model that discriminates between the polar head and the lipid core region [75–77].

The TIP3P water model [78] is consistently used in all the simulated systems. Molecular Dynamic simulations is visualized and analyzed by using the VMD code [79]; the most relevant non-covalent interactions (NCI) throughout the MD trajectories were analyzed and depicted with NCIPlot code [80]. The study of the gradient of the electronic density clearly differentiates NCIs in terms of steric clashes, dispersion and hydrogen bonding.

4.1.3. Electronic Structure Calculations

Gaussian 09 program package with Density Functional Theory (DFT) B3LYP and 6-31G(d) basis set level of theory is used to perform single point energy calculations and geometry optimizations. The potential energy surface scan to parameterize the mTHPC force field and the conformational analysis were performed with the same level of theory, the energies along the scan have also been estimated using the second order Moller–Plesset perturbation theory (MP2).

Vertical electronic excitations from ground state is obtained by using Time-Dependent Density Functional Theory (TD-DFT) in order to simulate the absorption spectra. The choice of the exchange–correlation functional and basis set is further justified by a benchmark on the calculation of the vertical excitation energies from the ground state equilibrium geometry. The selection of functional has more profound effect while the effect of the basis set on the excitation energies appears to be negligible. To be more specific, ωB97xd and M06-2X bring forth the correct separation of the Qx and Qy bands, in the red wavelengths region, meanwhile B3LYP only yields an unresolved broad band. Therefore, ωB97xd/6-31G(d) clearly revels the best compromise between computational cost and accuracy, meanwhile for the Zn atom is defined with the 6-31+G(d,p) basis set due to better definition. All UV-Vis absorption spectra were generated from the convolution of vertical excitations from 50 to 100 snapshots randomly extracted from the Molecular Dynamic simulations trajectories. The convolution of the vertical excitation energies and oscillator strengths was performed using Gaussian functions of full width at half-length (FWHL) of 0.15 eV. All the details regarding the calculations are stated in Figure 4.1 for Temoporfin and for the detailed choices for the calculations for Zn-Ar is stated in Table 4.1 for Zn-Ar.

Table 4.1: Details of the Zn-Ar simulations

1. Zn-Ar in vacuum	**Simulation**
Method	Classical MD
Time (ns)	100 ns
Timestep (fs)	2.0
Temperature (K)	300
Ensemble	NPT Nosé-Hoover Langevin barostat Langevin thermostat
2. Zn-Ar in water	**Simulation 3**
Method	Classical MD
Box size (A)	65.4 54.6 50.1

Table 4.1 continued from previous page

1. Zn-Ar in vacuum	**Simulation**
Time (ns)	100 ns
Timestep (fs)	2.0
Temperature	300
Ensemble	NPT Nosé-Hoover Langevin barostat Langevin thermostat

a) mTHPC in vacuo

	Simulation 1	Simulation 2	Simulation 3
Method	QM MD 6-31G/B3LYP	Classical MD	Classical MD
Time (ps,ns)	60ps	100 ns	100ns
Timestep (fs)	0.5	2.0	2.0
Temperature (K)	300	300	300
Ensemble	NPT	NPT Nosé-Hoover Langevin barostat[4,5] Langevin thermostat[6]	NPT Nosé-Hoover Langevin barostat Langevin thermostat

b) mTHPC in water

	Simulation 1	Simulation 2	Simulation 3
Method	QM/MM MD 6-31G/B3LYP	Classical MD	Classical MD
Time (ps,ns)	60ps	100ns	100ns
Box size (Å)	35.0 35.2 31.3	34.9 34.2 28.1	35.0 35.2 31.3
Timestep (fs)	0.5	2.0	2.0
Temperature (K)	300	300	300
Ensemble	NPT	NPT Nosé-Hoover Langevin barostat Langevin thermostat	NPT Nosé-Hoover Langevin barostat Langevin thermostat

c) mTHPC:TM-β-CD complex in water

	Simulation 1	Simulation 2	Simulation 3
Method	QM/MM MD 6-31G/B3LYP	-	Classical MD
Time (ps,ns)	10ps	-	100ns
Box size (Å)	90.3 84.3 84.4	-	90.3 84.3 84.4
Timestep (fs)	0.0005	-	2.0
Temperature (K)	300	-	300
Ensemble	NPT	-	NPT Nosé-Hoover Langevin barostat Langevin thermostat

d) mTHPC:POPC in water

	Simulation 1	Simulation 2	Simulation 3
Method	-	-	Classical MD
Time (ns)	-	-	100 ns
Box size (Å)	-	-	81.0 81.0 138.0
Timestep (fs)	-	-	2.0
Temperature (K)	-	-	300
Ensemble	-	-	NPT Nosé-Hoover Langevin barostat Langevin thermostat

Figure 4.1. Computational details of mTHPC for each environment. Simulation 1 is for Quantum Mechanics, Simulation 2 is for oldFF classical Molecular Dynamic Simulations and Simulation 3 is for the newFF classical Molecular Dynamics Simulations.

4.2. Investigation of Temoporfin (mTHPC)

Structural and optical properties of temoporfin (mTHPC) are investigated in molecular environments of increasing complexity. The interaction of mTHPC is explored in water, in TM-β-CD, and in lipid bilayer is modelled by using molecular simulations, and eventually compared with experimental and newly designed zinc coordinated photosensitizer (Zn-Ar). Different levels of theory are employed, and the effects of the molecular environment is discussed.

mTHPC contains four phenol rings encircled around the core chlorin ring which is crucial for optical properties of the chromophore, meanwhile the phenol rings are functionalized to induce the specific intermolecular interactions with the environment. Moreover, encapsulation of temoporfin with TM-β-CD complex affects the orientation and flexibility of phenol substituents. Therefore, proper parametrization of the force field to obtain this distinct phenomena and the rotational flexibility of the phenol substituents with respect to the chlorin core is of utmost importance.

The simulations were initially conducted with a force field from previous study to investigate mTHPC [81], which will be called "oldFF" in this thesis. Then, the forces on the phenol rings of the temoporfin is reduced to zero and new parameterized mTHPC is analysed, which will be referenced to as "newFF" in this thesis and compared with the oldFF. Lastly, the newFF is verified through the QM/MM MD calculations and the results are reported.

4.2.1. Dihedral Angle Distribution Analysis of Temoporfin (mTHPC)

Rotation of phenolic rings are portrayed with the dihedral angle distribution of mTHPC (Figure4.2). The phenolic rings rotation is anticipated to be in wider range in gas phase and in water, however the observation of full rotation of the phenolic rings is not possible due to the clashes between phenyl hydrogens and chlorin core. The case is different for the mTHPC:TM-β-CD complex due to large steric hinderance. The

naming convention for *intra* and *inter* phenolic rings are determined according to their placement in the cyclodextrin unit. *intra* and *inter* phenolic rings are investigated in gas, in water and popc lipid bilayer as well.

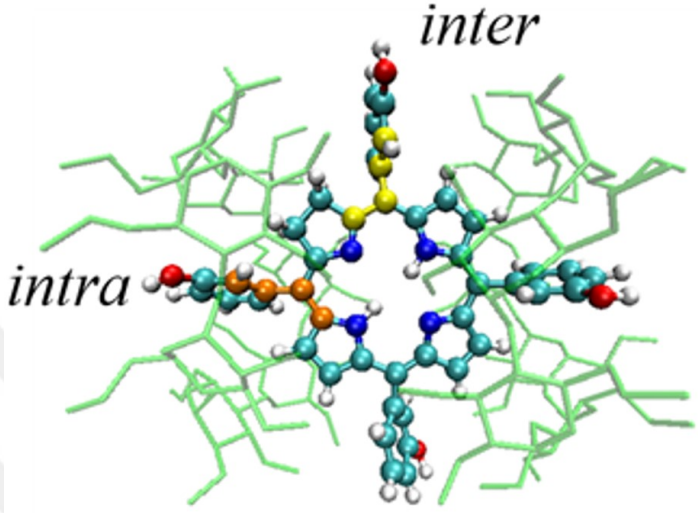

Figure 4.2. Encapsulated temoporfin in TM-β-CD complex with *intra* (in orange) and *inter* (in yellow).

4.2.1.1. mTHPC in vacuum. Dihedral angle distributions of mTHPC have been investigated through the calculations conducted by Molecular Dynamics and Quantum Mechanic/Molecular Dynamics simulations. Calculations from QM scan in a vacuum for Temoporfin's peripheral dihedral angle, performed both at DFT and MP2 level of theory Figure 4.3. The results verify a large degree of freedom of the phenolic group as seen by the nearly flat potential energy curve in the $\pm 60 - 120°$ region. The sharp increase in the potential energy around 0° and 180° is due to steric repulsion with the core and is indicative of the emergence of two distinct conformers. Meanwhile the core stability is also investigated with classical molecular dynamics simulation and QM/MM MD shown in Figure B.1.

To properly represent the free rotation of the phenol rings were investigated with classical force field for mTHPC by setting the force constant to zero. The results for the distribution of the dihedral angles in the different environments obtained with the

classical force field match remarkably with the ones of the QM/MD. Note that the mTHPC FF was parametrized to better represent the PS in confined environments, hence, it is somewhat expected that its performance will be less adequate in vacuum and in solution where the rotational flexibility is larger. These degrees of freedom are critical in describing the global vibration of the drug and may have an influence on the observed optical properties.

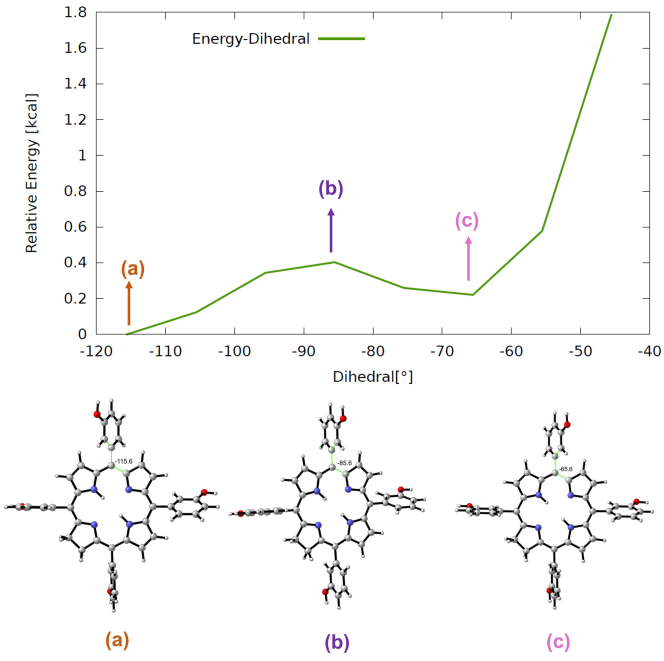

Figure 4.3. Rotational free energy (M062X/6-31+G(d)) profile for a dihedral scan. The geometry of the molecule in the three points a, b and c is displayed in the bottom panel.

The out-of-plane normal modes is be responsible for the red-shift of the absorption spectra with respect to vertical transitions calculated from the ground state geometry only Figure 4.3 due to the significant destabilization of the ground state rather than the excited state, as is common for similar π-conjugated systems [47, 82–86]. Although the influence of the rotation of the peripheral substituents on the absorption spectral maxima is expected to be marginal, it may, nonetheless, induce a broadening of the absorption and emission bands, and more notably, may have a key role in inducing thermal quenching of the luminescence. While the possibility to take into account

the out-of-plane deformation effects via a reasonable sampling of the conformational space is well established and has been thoroughly demonstrated in similar systems [82, 83, 87, 88], the effects of the peripheral dihedral rotations require much deeper attention, due to their strong non-harmonic behaviour.

In order to prove these, firstly, the dihedral angles of oldFF and newFF were calculated by the classical MD simulations were analysed and compared. The range between the distribution of the dihedral angle of the phenol ring is displayed as wider compared to the oldFF. The newFF can scan wider more than 20° meanwhile the rotation of the phenol rings of temoporfin, which is parametrized by oldFF prefers to stay rather than rotating Figure 4.4. So, removing the force from the phenol rings provides better peripheral dihedral rotations, and at the end, it is expected to red-shift the absorption spectra.

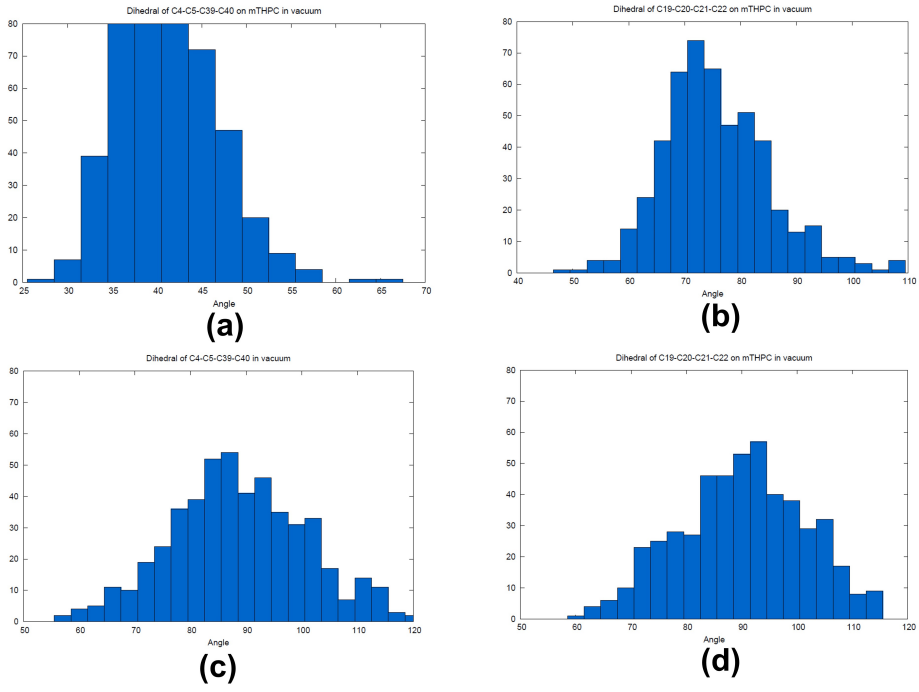

Figure 4.4. Distribution of the *inter* (a) oldFF (c) newFF and *inter* (b) oldFF (d) newFF dihedrals of mTHPC in vacuum extracted from classical MD.

In order to validate the new parameterized force field, the QM MD simulations were conducted and the dihedral angle of the phenol rings were analysed. The temoporfin is treated at the QM level, and a dramatic change is observed as mTHPC is close to complete the full rotation Figure 4.5. However, it is expected that the full rotation is impossible due to the atomic clashes between phenol rings and the chlorin core atoms.

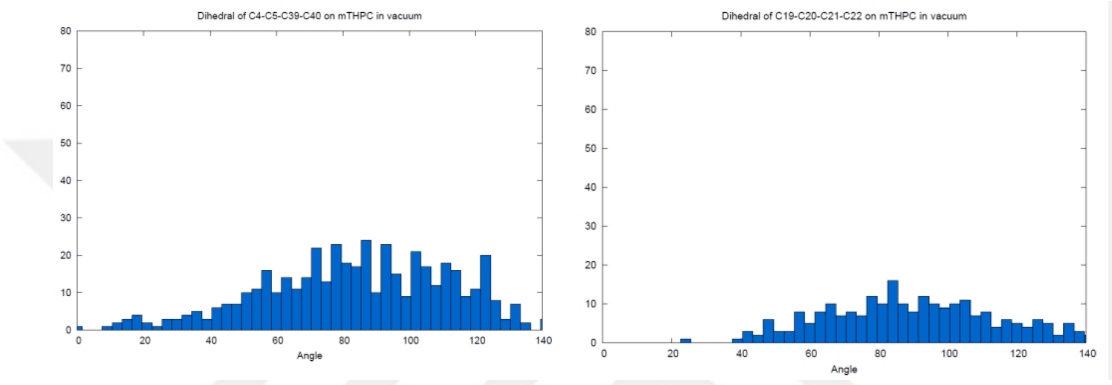

Figure 4.5. Distribution of the inter (left) and intra (right) dihedrals of mTHPC in vacuum during QM MD calculations.

4.2.1.2. mTHPC in water. Distribution of dihedrals for mTHPC in water is analysed with the same procedure as in gas. The compared results from oldFF vs newFF in water is also same as in gas and newFF gives better results.

For the QM/MM MD simulations, it needs to be stated again that mTHPC is treated with QM, meanwhile the water molecules are treated in MM level. The results from the mTHPC in water for QM/MM MD simulations have a wider range compared to the classical Molecular Dynamics simulations, which is expected due to the higher description of the electronic attitude of atoms and molecules Figure 4.6. Additionally, distribution of the mTHPC in water is narrower than the results from gas in range of 10-20°. This behavior could be explained straightforwardly with lack of the freedom of the phenolic rings in water due to steric clashes.

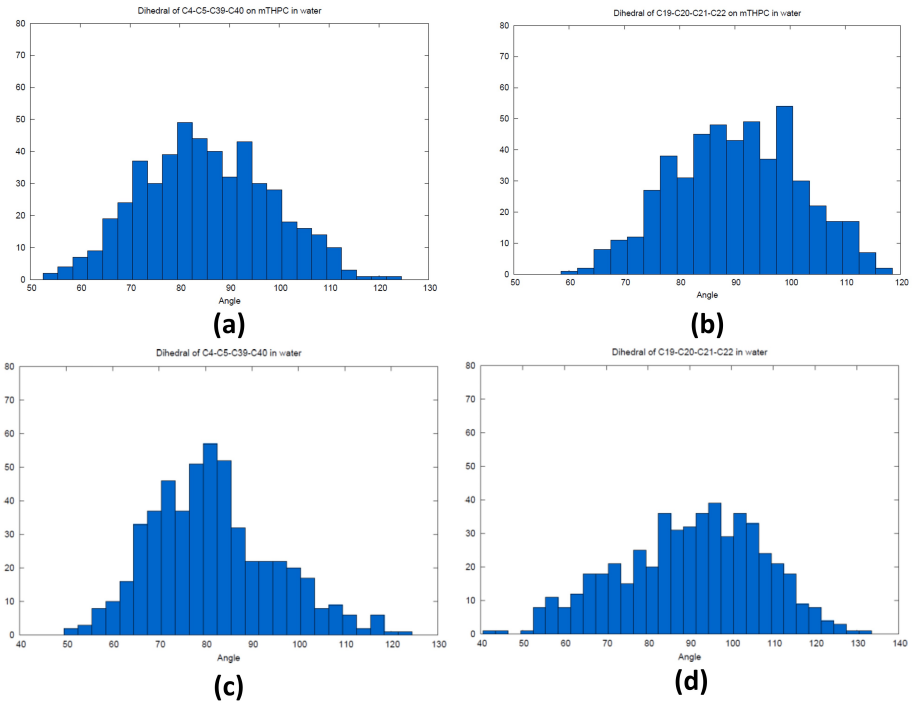

Figure 4.6. Dihedral distribution of the inter (left) and intra (right) dihedrals in mTHPC in water during Classical MD (top) QM/MM MD simulations (bottom).

The stability of the core structure of mTHPC in water Figure B.2 shows that the mTHPC core from oldFF is stabilized after 20 ns meanwhile newFF mTHPC core is equilibrated from the beginning of the simulation. Even the QM/MM MD simulation was for 60 picoseconds, the results indicated the stability of the chlorin core structure.

4.2.1.3. mTHPC:TM-β-CD complex. From now on, the newFF results will be compared with the results from the QM/MM MD. Temoporfin-cyclodextrin complex which is abbreviated as mTHPC:TM-β-CD complex, presents steric hindrance due to the encapsulation. As seen in Figure 4.7, two of the phenolic groups of mTHPC are located inside of the cyclodextrin pockets (*intra*), while the other two occupies the hydrophobic region between the two cyclodextrins (*inter*). Even though the mobility is inevitably decreased compared to the water case Figure 4.6; the dramatic difference between the *intra* and *inter* cases of phenolic rings is also observed Figure 4.7. This is due to the highly constrained interior of the cyclodextrin core that is explored by the intra-phenol

moeity.

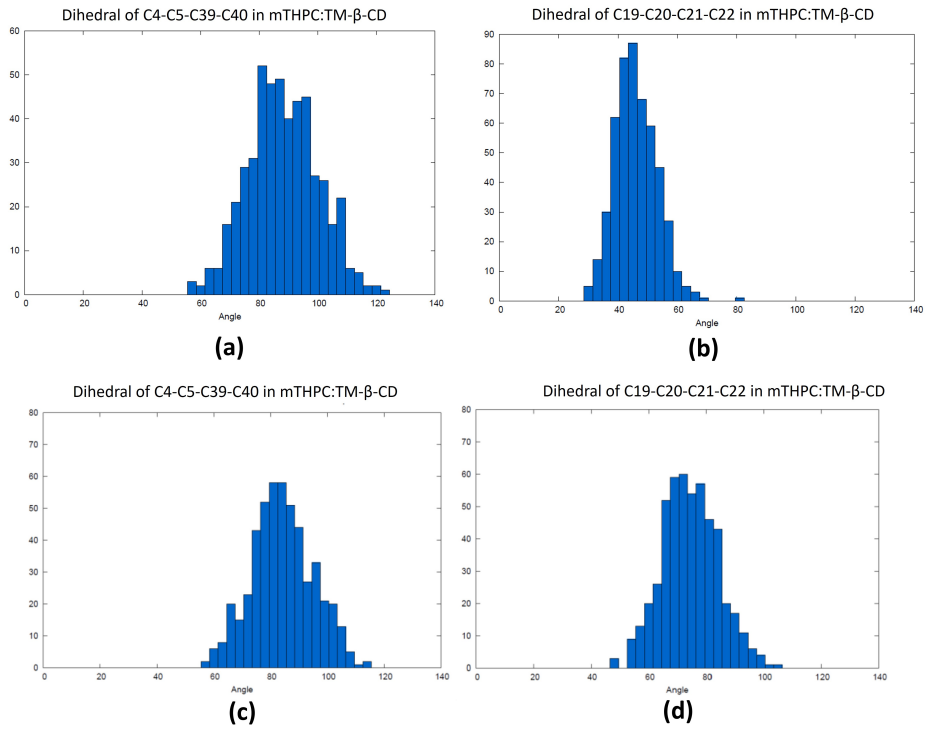

Figure 4.7. Distribution of the inter (a) newFF (c) QM/MM MD and intra (b) newFF (d) QM/MM MD dihedrals of mTHPC in water extracted from Classical MD.

The stability of the chlorin core structure of mTHPC:TM-β-CD complex in water Figure B.3 shows that the mTHPC core from newFF is stabilized from the beginning of the simulation. Even though QM/MM MD simulation is for 20 ps, the results indicate of the stability of the core chlorin structure. Additional investigation is conducted to understand the stability of the carbon atoms of the phenol rings inside of the two TM-β-CD(*intra*) and between the two TM-β-CD complexes(*inter*) stated in the Figure B.4.

4.2.1.4. mTHPC:POPC. In the obtained most stable configuration, mTHPC is positioned around the polar head regions, and more precisely, at the interface between the phosphate and the fatty acid hydrophobic core. Indeed, mTHPC is more exposed to the lipid environment than to the water bulk. This behaviour is not totally unexpected and can be traced back to the concomitant presence of a hydrophobic core and phenol groups that may develop specific non-covalent interactions with the polar head regions. However, the position of mTHPC is most favorable for PDT purposes. Indeed, while O_2 will permeate the membrane due to its hydrophobic nature as also revealed by MD simulations [89], it will also have a non-negligible concentration in the region occupied by the photosensitizer. In addition, our density profile also shows that mTHPC partially overlaps with the position of the lipid carbon–carbon double bond. This fact indicates that $^1O_2$ will be produced in close proximity to its reactive target, hence minimizing the quenching probability (Figure 4.8).

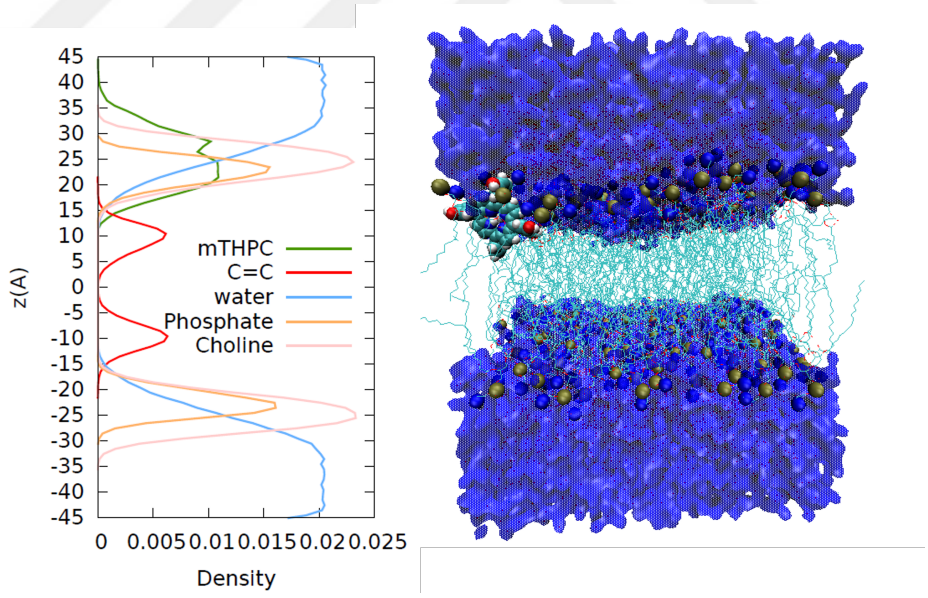

Figure 4.8. mTHPC contacts with double bond C-C of POPC lipid bilayer where the singlet oxygen generation occurs.

It has also been reported that photosensitizers, also porphyrin based, may exert photopermeabilization of the lipid membrane via an alternative contact dependent mechanism, that involves electron abstraction from solvent or lipids [90, 91]. Although further studies, including the modelling of additional membrane components, such as cholesterol, should be needed to confirm this scenario, our density profile, and the partial overlap identified, claims in favour of the possibility of this photophysical route, concerning the chromophore positioning and the key geometrical factors.

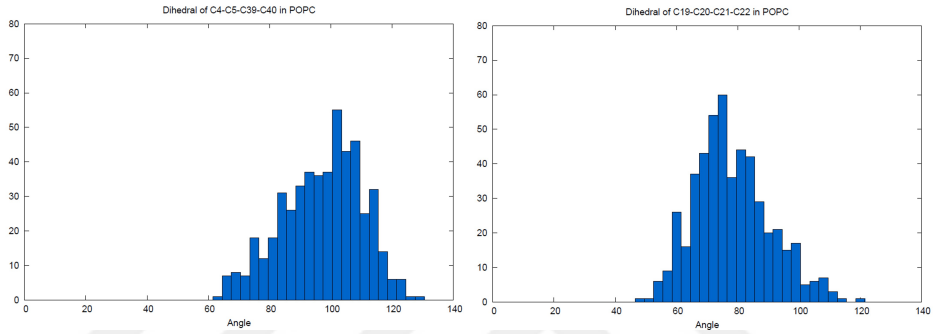

Figure 4.9. Distribution of the inter (left) and intra (right) dihedrals for mTHPC in POPC lipid during Classical MD simulation.

The Figure 4.9 displays the limited rotation of the phenyl rings inside of the bulk of lipid bilayer between 60° range. The phenomena is expected due to the clashes between phenyl rings of mTHPC and surrounding water and lipid chains.

The stability of the core chlorin structure of mTHPC in POPC lipid bilayer Figure B.5 shows that the mTHPC core from newFF is stabilized from the beginning of the simulation.

4.2.2. Absorption Spectra Analysis of Temoporfin (mTHPC)

Before the absorption spectra analysis started, the benchmark calculations are conducted to determine the appropriate basis set and the functional to use. B3LYP M062x, ωB97xd are the chosen functionals due to their accurate results for the TD-DFT calculations. [92] As a basis set, 6-31g, 6-31g(d), 6-31g(d,p) and 6-311g is explored for each of the functionals.

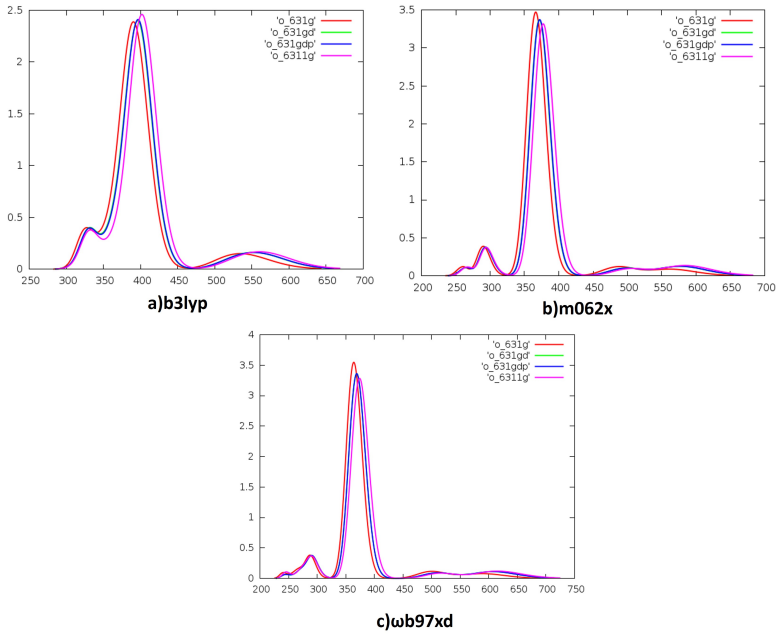

Figure 4.10. Benchmark to determine the functional and the basis set.

Results in the Figure 4.10 indicated that the ωb97xd gives the better characterization of the Q band in the visible region as displaying the Qx and Qy bands separately. The perspective of the basis set, 6-31g(d), 6-31g(d,p) have overlapped and given the similar results meanwhile 6-31g has given the poorer, blue-shifted result. Even though the result of 6-311G is better than rest of the basis sets compared, the computational cost has taken into consideration and 6-31G(d) is preferred.

The investigation of absorption spectra in each environment compared between the absorption spectra calculated as the convolution of vertical transitions from a series of snapshots obtained by sampling mTHPC's conformational space with either a QM/MM approach, in which the whole chromophore is treated quantum mechanically, or a MM approach, in which the dynamics of the chromophore is described by a force field (classical MD).

4.2.2.1. mTHPC in vacuum. The absorption bands is displayed in the 500–680 nm region, corresponding to the Q-bands, as well as the more intense Soret bands in the

blue region. It is evident from the analysis of the QM based MD simulation of mTHPC in the gas phase Figure 4.11 that two low-energy large-amplitude degrees of freedom dominate the conformational space: the out-of-plane deformation of the conjugated ring system and the rotation of the peripheral phenolic units.

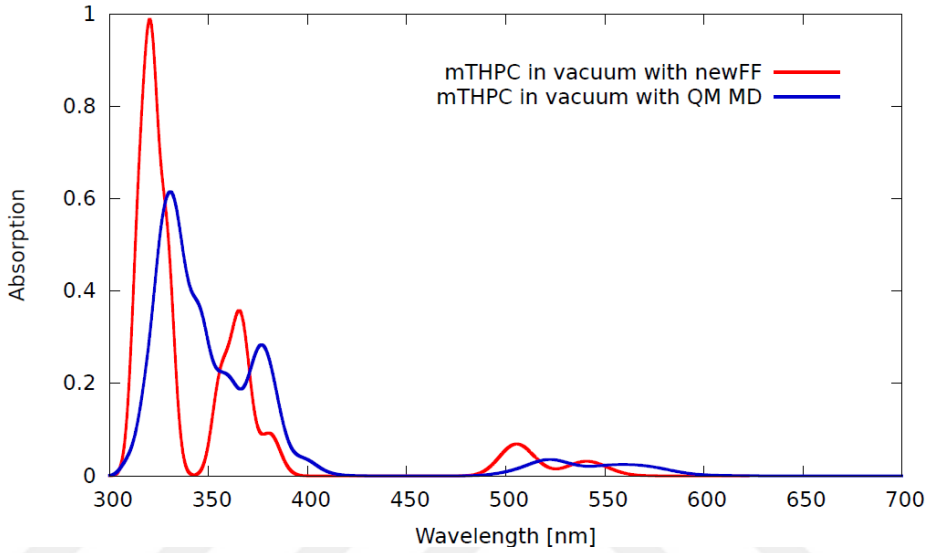

Figure 4.11. Absorption spectra of mTHPC in vacuum calculated by classical MD and QM MD.

4.2.2.2. mTHPC in water. The absorption bands are shown in the 500–680 nm range, which corresponds to the Q-bands, as well as the more intense Soret bands in the blue range. The conformational space is dominated by two low-energy large-amplitude degrees of freedom: out-of-plane deformation of the conjugated ring system and rotation of the peripheral phenolic units.The result from QM/MM MD shows a more red-shift on the Q-band compared to classical MD.

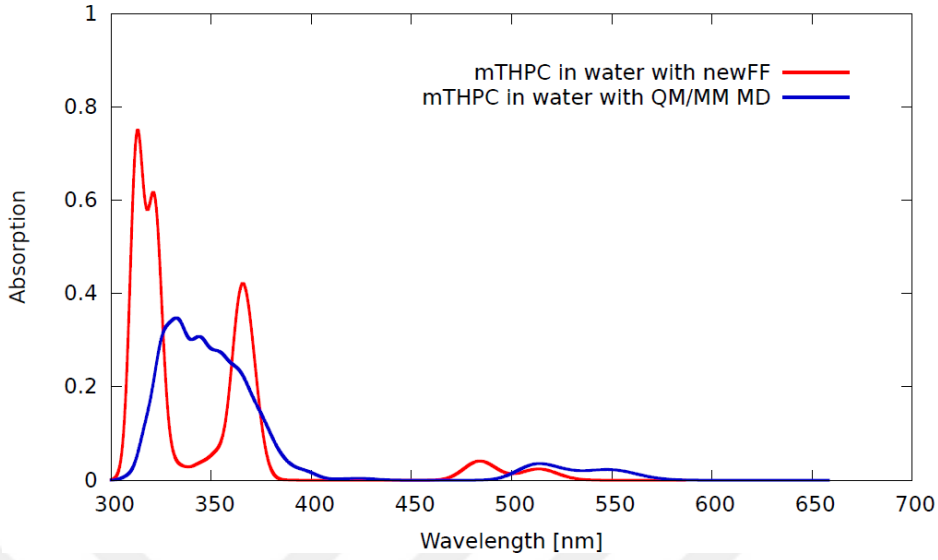

Figure 4.12. Absorption spectra of mTHPC in water calculated by classical MD and QM/MM MD.

4.2.2.3. mTHPC in TM-β-CD. The effect of the molecular surrounding, and in particular of the embedding in confined environments, such as cyclodextrin, should be properly taken into account.The phenol rings in the macromolecular complex as opposed to the gas phase or solution may also offer an additional reason for the enhancement of fluorescence observed in the host complex. The free rotation of the peripheral moieties would offer a further non-radiative decay pathway that will lead to the deactivation of the excited state. Indeed, the restricted intramolecular rotation has been recognized as a cause of the fluorescence enhancement in different organic luminophores [93,94]. As it is the case for diverse fluorophores [95–97], the aggregation of chromophores,and hence the formation of dark excitonic states, could also be considered as a supplementary phenomenon leading to fluorescence quenching in solution.

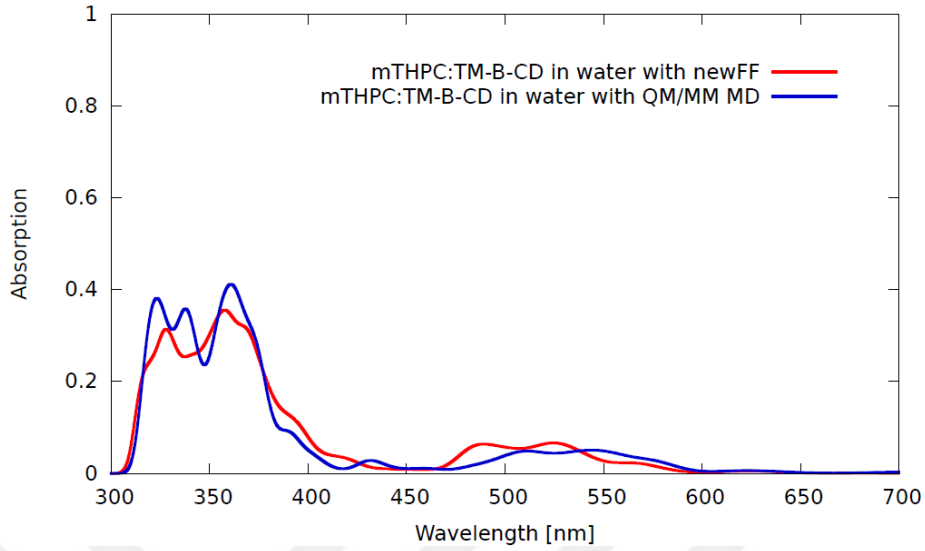

Figure 4.13. Absorption spectra of mTHPC complex with TM-β-CD in water calculated by classical MD and QM/MM MD.

The agreement between the different levels of the theory is confirming the validity of the chosen approach, the only difference being the slightly more red shifted Q-band obtained with the QM/MM. Interestingly, the Q-band region also appears more sensitive to the specific chemical environment, in particular for the absorption spectrum of the mTHPC:TM-β-CD. Indeed, in this case, the inversion of the intensity between the Qx and Qy Soret bands observed experimentally, constituting one of the spectroscopic signatures of complex formation, is clearly identified and nicely reproduced by the full classic and the hybrid sampling protocol.

4.2.2.4. mTHPC:POPC. The robustness and precision of our force field parameterization that has been validated by means of different levels of theory and proven to reproduce both the structural parameters and the optical properties of mTHPC in different environments, we move to examine the interaction, between the chromophore and a lipid bilayer. Indeed, the mode of action as a PDT drug should involve the disruption of the cell membrane induced by the activated $^1O_2$ following the absorption of light. The results of the MD simulation are reported in Figure 4.8 in the form of the density profile along the membrane axis for the main functional group and pictorially

using a representative snapshot.

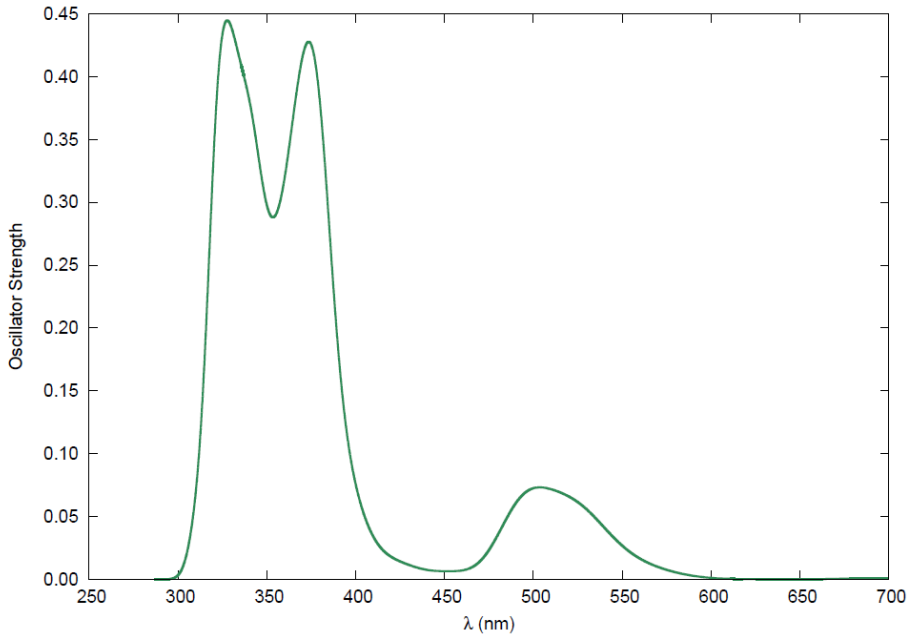

Figure 4.14. mTHPC absorption spectra in POPC lipid bilayer through 100 ns MD simulation.

At the beginning of the simulation the photosensitizer is placed in bulk water and unsurprisingly, due to its hydrophobic nature, mTHPC develops favorable interactions with the lipid membrane with a persistence time exceeding hundreds of ns. The absorption spectrum calculated in the POPC interface is also reported in Figure 4.14 and shows that most of the characteristic spectral features are maintained. Indeed, both the Q and the Soret bands are clearly distinguishable, and interestingly, in contrast with what was observed in the case of the mTHPC:TM-b-CD complex, no inversion between the Qx and Qy band is observed. However, the energy differences between the two bands are underestimated by our computational approach, as compared to experiment. This difference could mostly be ascribed to the neglect of purely quantum vibronic coupling through the explicit calculation of Franck–Condon parameters [98,99]. However, such an approach, despite some interesting recent developments, is still far from being standardized [100].

4.2.3. Specific Interactions of mTHPC:POPC

To better characterize the factors influencing the stability of the persistent aggregate evidenced in the MD trajectory, we performed a detailed analysis of the specific interactions taking place between mTHPC and the lipid constituents. As reported in Figure 4.15, in addition to dispersion interactions typical of hydrophobic compounds, the formation of specific interactions mainly involving hydrogen-bonding between the phenol groups and the negatively charged phosphates, contributes to locking the chromophore at the interface region.

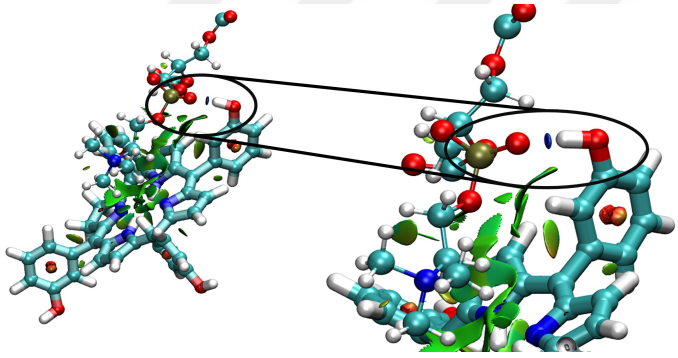

Figure 4.15. Hydrogen bonding between hydrogen of the temoporfin phenol and the phosphate oxygen at the PC part of the POPC lipid.

This interaction, as well as its persistence, is confirmed by the structure of the radial distribution function presented in Figure 4.16, for the involved phenolic hydroxyl and the phosphate oxygen groups. The sharp peak at around 1.6 Å is very indicative of a typical and persistent hydrogen bond. The same conclusions can be drawn from the NCI plots for some representative snapshots. The features of a hydrogen bond formation, represented by the concentrated green circle around the phosphate and phenol group, are indeed clearly evident in the zoom of Figure 4.16.

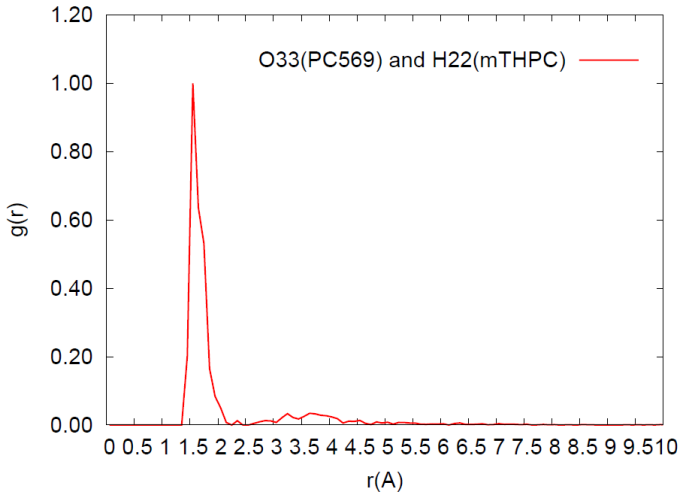

Figure 4.16. Hydrogen bonding between hydrogen of the temoporfin phenol and the phosphate oxygen at the PC part of the POPC lipid.

Although the hydrogen bonding pattern was somewhat expected, other non-covalent interactions are also pertinent, namely, the cation–π interactions between the aromatic mTHPC core chlorine and the positively charged choline in the lipid head groups are clearly evidenced both by the radial distribution function and by the NCI plot Figure 4.17.

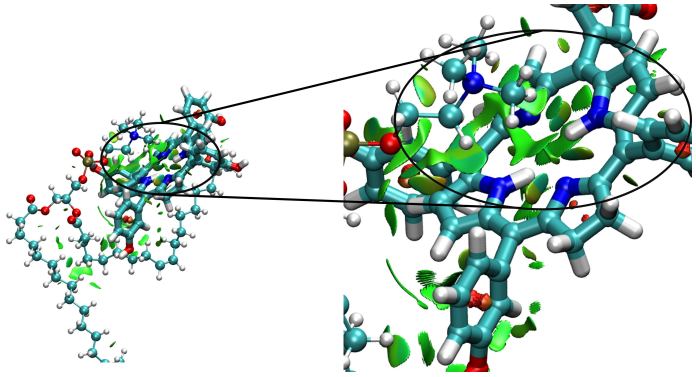

Figure 4.17. Cation-π interaction between the temoporfin chlorine ring with the N atom at the PC side of the POPC lipid.

The structure of the radial distribution function for the relevant cationic nitrogen of POPC and chlorin core, shown in Figure 4.18, confirms this connection as well as its durability. A typical and persistent cation-π is indicated by the steep peak at approximately 4 which supports the noncovalent molecular interaction between the face of an electron-rich π systems [101].

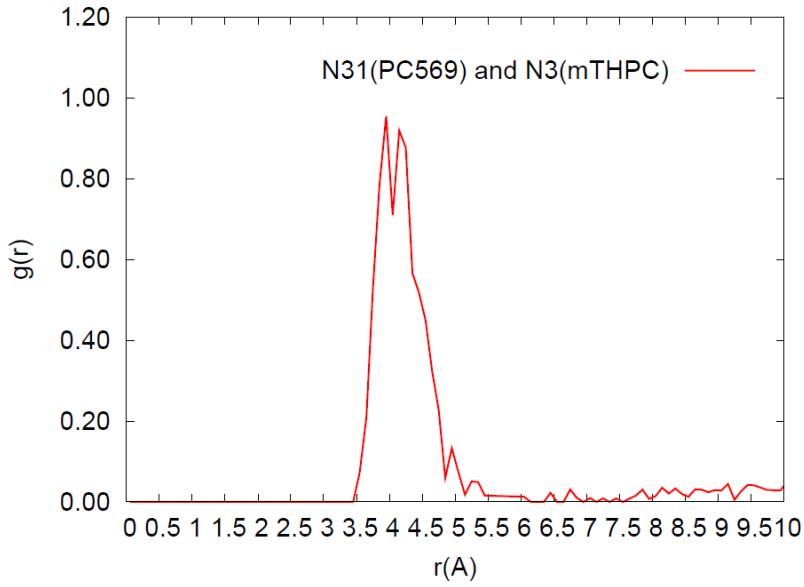

Figure 4.18. Cation-π interaction between the temoporfin chlorine ring with the N atom at the PC side of the POPC lipid.

4.3. Investigation of Metal Coordinated Chlorin (Zn-Ar)

In this section, the results from the zinc coordinated chlorin derivative photosensitizer candidate(Zn-Ar) will be investigated thoroughly included dihedral angle distribution of the phenyl ring of Zn-Ar in each environment, UV-Vis spectra in vacuum and in water.

4.3.1. Dihedral Angle Analysis of Metal Coordinated Chlorin (Zn-Ar)

The rotation of the pyrroline ring around the chlorin core structure is investigated due to the fact that these degrees of freedom are critical in describing the global vibration of the drug. In order to do this, C8-C14-C27-C30 dihedral is selected and the dihedral angle distribution is examined as shown in Figure 4.19.

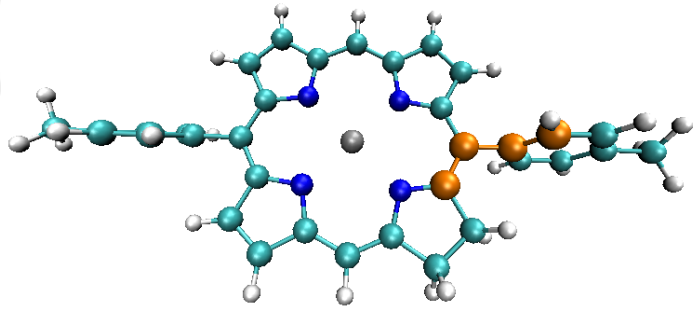

Figure 4.19. Dihedral angle which is indicated with an orange color of the carbon atoms of the pyrroline ring around the chlorin core of Zn-Ar.

4.3.1.1. Zn-Ar in Vacuum. Dihedral angle distributions of Zn-Ar have been investigated through the calculations conducted by classical MD simulations. The scan for the peripheral dihedral angle of Zn-Ar in vacuum, are performed (Figure 4.20). The results results that a large degree of freedom of the phenolic group as seen nearly in the $\pm 50 - 130°$ region. Absence of rotation on less than 50° and more than 120° is due to steric repulsions between the core chlorine and the phenyl ring hydrogens.

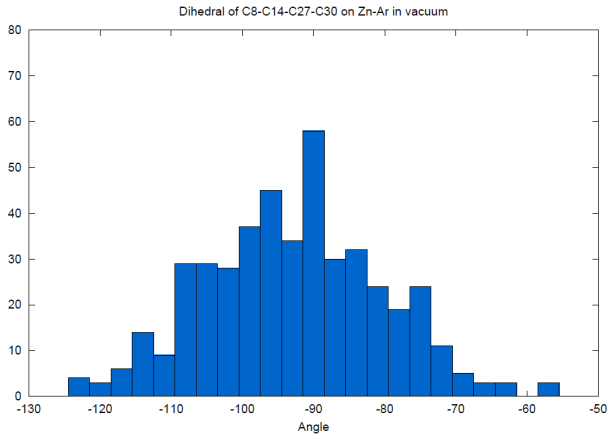

Figure 4.20. Dihedral angle distribution of atoms for phenyl ring positioned near pyrroline

4.3.1.2. Zn-Ar in water. Distribution of dihedrals for Zn-Ar in water has a wider range compared to the phenyl ring rotation in vacuum. The peak which can be clearly seen in vacuum at 90° is expanded around $\pm 80 - 100°$ in water.

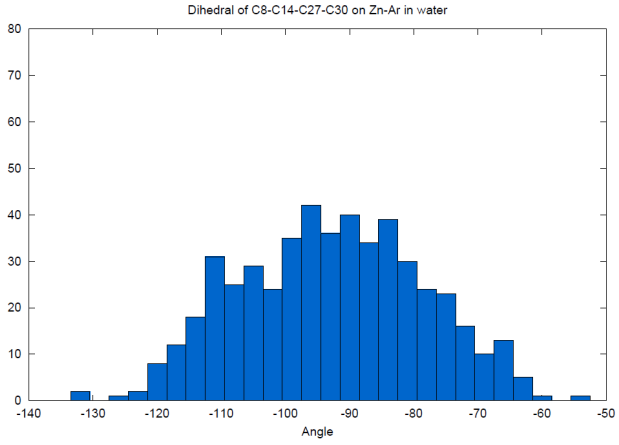

Figure 4.21. Dihedral distribution of the selected atoms on phenyl ring of chlorin in water.

4.3.2. Absorption Spectra Analysis of Metal Coordinated Chlorin (Zn-Ar)

4.3.2.1. Zn-Ar in vacuum. The absorption spectra of Zn-Ar is obtained from 50 snapshots from the Molecular dynamic simulation and is presented the expected results for the chlorin based chromophores. The absorption bands in the 500–680 nm region, corresponding to the Q-bands, as well as the more intense Soret bands in the blue region. In addition, the effect of metal coordination with the chlorin ring clearly observed via red shift.

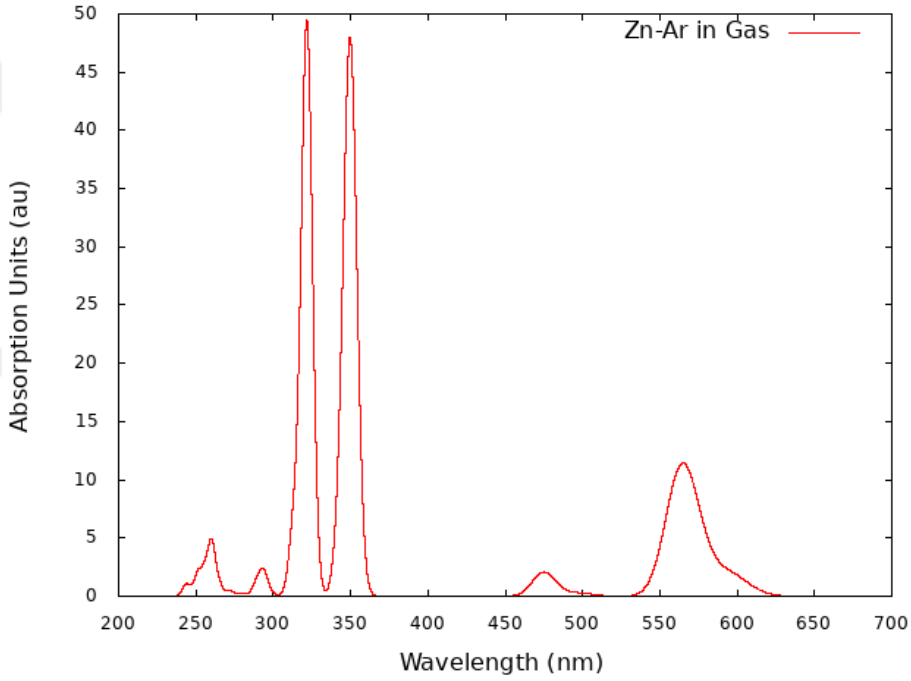

Figure 4.22. Absorption Spectrum of the Zn-Ar in gas.

4.3.2.2. Zn-Ar in water. The absorption spectra of Zn-Ar are obtained from 47 snapshots from the Molecular dynamic simulation. The absorption bands in the 800-900 nm region, effect of the metal coordination displays the bathochromic shift effectively. The effect of the π-conjugation of the zinc with the chlorin core is observed with the higher molar absorptivity compared to the free base chlorins. Meanwhile, compared to the Zn-Ar in gas vs in water, dramatic change for the absorption peak is detected, which is more than 200 nm difference. The result indicates that Zn-Ar could be a great promising photosensitizer agent which will be easily carried in the blood.

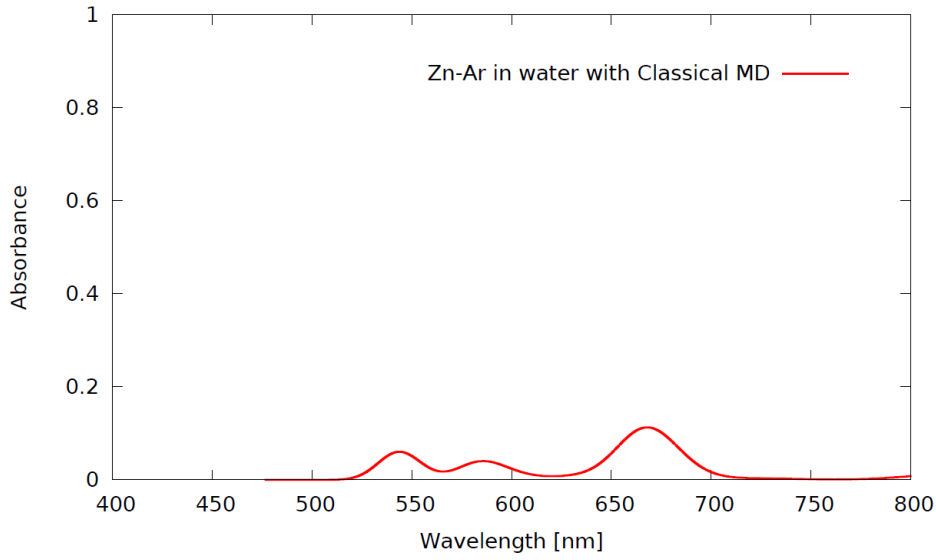

Figure 4.23. Absorption Spectrum of the Zn-Ar in water.

4.4. Comparison of mTHPC with Zn-Ar

In this section, the results from the zinc coordinated chlorin derivative molecule (Zn-Ar) will be compared with the results of temoporfin from classical MD simulation in gas and in water with the experimental results.

4.4.1. Absorption Spectra Comparison of mTHPC and Zn-Ar

In biological systems, chromophores' optical properties are greatly influenced by their interactions with their surroundings (nearby protein residues, membrane, water), and the complexity of this interaction is, in most situations, at the root of the photoactive proteins' functional diversity. When chromophore excitation energies are compared to their absorption in solution or gas phase, certain interactions with the environment typically result in a substantial shift [102]. Especially the coordination with metal induces the red-shift in the absorption due to the π-conjugation of planar chromophore-metal complex, which results in a 35 nm gap between the Q-band of absorption spectra between mTHPC and Zn-Ar in vacuum.

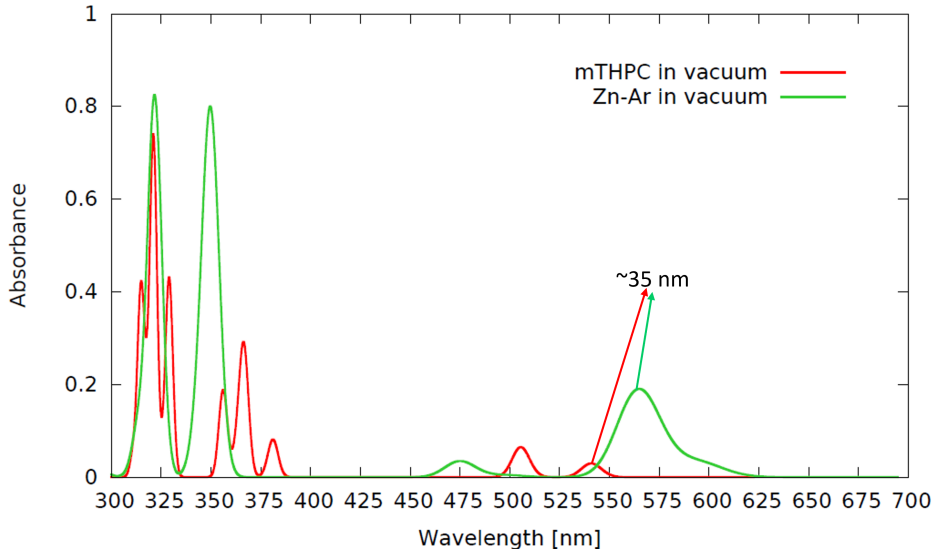

Figure 4.24. Absorption Spectra of the Zn-Ar and mTHPC in vacuum.

The QM/MM MD calculation gives the bathochromic shift compared to the Classical MD result and gives more coherent result according to the reference mTHPC in ethanol.

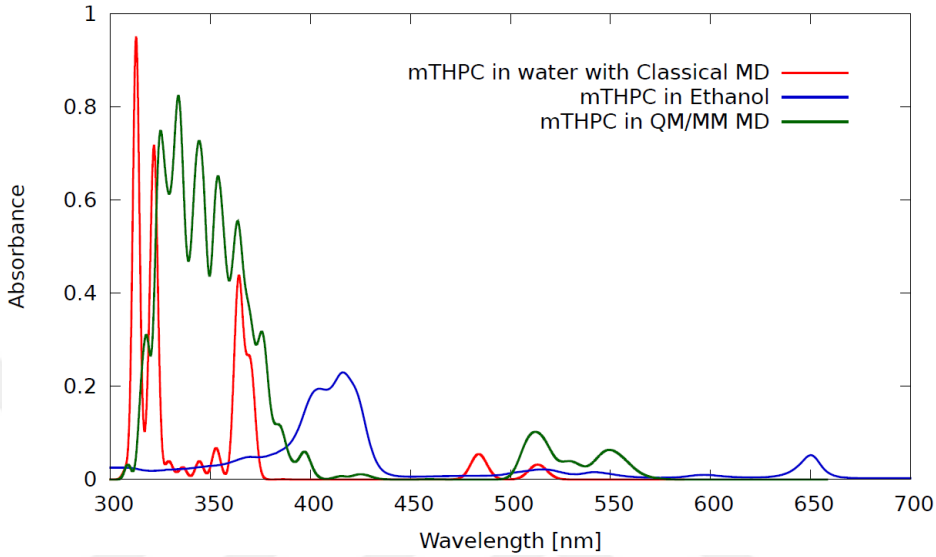

Figure 4.25. Absorption Spectra of the mTHPC in water from Classical MD and QM/MM MD vs mTHPC in ethanol experimental result.

The absorption spectra of Zn-Ar in water which is calculated by Classical MD gives the absorption at 660 nm.

The results effectively proves that firstly, the chlorin core coordination with Zn induces the π conjugation, and secondly the rotation ability of the phenyl ring around 70° disrupts the π-π stacking of the π conjugated chlorin core.

5. CONCLUSION

In this thesis, the detailed analysis of the structural and optical properties of two compounds are discussed a) known photosensitizer as mTHPC and b) Zn-Ar. Temoporfin, which is already clinically used for PDT purposes, is simulated in different complex environments, including a cyclodextrin-based encapsulated drug delivery agent, and a model lipid bilayer.Zn-Ar is also a promising candidate for the future application of photodynamic therapy. The results show that the confined environment of the cyclodextrin induces a strong reduction of the mobility of the peripheral phenol rings. Furthermore, clear differences in the mobility degree appear for intra and inter substituents. The strong reduction of the phenyl ring rotation is also correlating well with the observed enhancement of the fluorescence quantum yield upon encapsulation.The results have also highlighted the formation of persistent aggregates between mTHPC and lipid membranes, with the sensitizer residing preferentially in the interface between the polar heads and the lipid core. This situation is favoured by interactions, such as the formation of hydrogen bonds and cation–π interactions with the polar heads that counterbalance the hydrophobic dispersion interactions developed with the lipid core. Interestingly, the position of the sensitizer represents one of the most ideal ones for PDT purposes, since it encompasses both the area of maximum oxygen concentration and a partial overlap with the position of the oxidizable lipid double-bond. In addition, the optical properties have been determined, including the sampling of the conformational space of the ground state, highlighting a rather marginal effect of the environment and the necessity to carefully parameterize the crucial force-field parameters.

The analysis of the Zn-Ar is completed in two different environments; namely vacuum and water, via classical molecular dynamic simulations. Even though the full scope analysis is not concluded, the results from Zn-Ar in solution concludes that new photosensitizer candidate has an absorbance ability in the red-light region, which makes it a new promising photosensitizer.

5.0.1. Future Remarks

In the future, study of mTHPC and Zn-Ar interactions with cyclodextrins and lipid membranes will be investigated in a two fold perspective. From the one side, the release from the encapsulating complex and the subsequent insertion in the lipid membrane will be studied by using enhanced molecular dynamics simulation techniques. In addition, the intersystem crossing, and hence the population of the triplet state manifold, for mTHPC and Zn-Ar in different environments will be studied including the possibility to perform QM/MM based non-adiabatic dynamics to quantitatively assess the quantum yield and timescales of the first event of the photosensitization chain.

REFERENCES

1. Wang, Y., J. Zhao, Z. Chen, F. Zhang, Q. Wang, W. Guo, K. Wang, H. Lin and F. Qu, "Construct of MoSe2/Bi2Se3 Nanoheterostructure: Multimodal CT/PT Imaging-Guided PTT/PDT/Chemotherapy for Cancer Treating", *Biomaterials*, Vol. 217, p. 119282, 2019.

2. Azizi, A., P. Shohrati, M. Goudarzi, S. Lawaf and A. Rahimi, "Comparison of The Effect of Photodynamic Therapy with Curcumin and Methylene Blue on Streptococcus Mutans Bacterial Colonies", *Photodiagnosis and Photodynamic Therapy*, Vol. 27, pp. 203–209, 2019.

3. Shen, J., Q. Liang, G. Su, Y. Zhang, Z. Wang, C. Baudouin and A. Labbé, "In Vitro Effect of Toluidine Blue Antimicrobial Photodynamic Chemotherapy on Staphylococcus Epidermidis and Staphylococcus Aureus Isolated from Ocular Surface Infection", *Translational Vision Science Technology*, Vol. 8, No. 3, pp. 45–45, 2019.

4. Zhang, L., Z. Ji, J. Zhang and S. Yang, "Photodynamic Therapy Enhances Skin Cancer Chemotherapy Effects through Autophagy Regulation", *Photodiagnosis and Photodynamic Therapy*, Vol. 28, pp. 159–165, 2019.

5. Hamblin, M. R., "Photodynamic Therapy for Cancer: What's Past is Prologue", *Photochemistry and Photobiology*, Vol. 96, No. 3, pp. 506–516, 2020.

6. Jarrett, P. and R. Scragg, "A Short History of Phototherapy, Vitamin D and Skin Disease", *Photochemical & Photobiological Sciences*, Vol. 16, No. 3, pp. 283–290, 2017.

7. Karppinen, T., L. Ylianttila, H. Kautiainen, T. Reunala, E. Snellman *et al.*, "Empowering Heliotherapy Improves Clinical Outcome and Quality of Life of

Psoriasis and Atopic Dermatitis Patients", *Acta Dermato-Venereologica*, 2015.

8. Zhang, J., C. Jiang, J. P. F. Longo, R. B. Azevedo, H. Zhang and L. A. Muehlmann, "An Updated Overview on The Development of New Photosensitizers for Anticancer photodynamic therapy", *Acta Pharmaceutica Sinica B*, Vol. 8, No. 2, pp. 137–146, 2018.

9. Yanovsky, R. L., D. W. Bartenstein, G. S. Rogers, S. J. Isakoff and S. T. Chen, "Photodynamic Therapy for Solid Tumors: A Review of The Literature", *Photodermatology, Photoimmunology & Photomedicine*, Vol. 35, No. 5, pp. 295–303, 2019.

10. Majumdar, P., R. Nomula and J. Zhao, "Activatable Triplet Photosensitizers: Magic Bullets for Targeted Photodynamic Therapy", *Journal of Materials Chemistry C*, Vol. 2, No. 30, pp. 5982–5997, 2014.

11. Buytaert, E., M. Dewaele and P. Agostinis, "Molecular Effectors of Multiple Cell Death Pathways Initiated by Photodynamic Therapy", *Biochimica et Biophysica Acta (BBA)-Reviews on Cancer*, Vol. 1776, No. 1, pp. 86–107, 2007.

12. Wang, Y.-Y., Y.-C. Liu, H. Sun and D.-S. Guo, "Type I Photodynamic Therapy by Organic-Inorganic Hybrid Materials: From Strategies to Applications", *Coordination Chemistry Reviews*, Vol. 395, pp. 46–62, 2019.

13. Montoya, S. C. N., L. R. Comini, M. Sarmiento, C. Becerra, I. Albesa, G. A. Argüello and J. L. Cabrera, "Natural Anthraquinones Probed as Type I and Type II Photosensitizers: Singlet Oxygen and Superoxide Anion Production", *Journal of Photochemistry and Photobiology B: Biology*, Vol. 78, No. 1, pp. 77–83, 2005.

14. Kou, J., D. Dou and L. Yang, "Porphyrin Photosensitizers in Photodynamic Therapy and Its Applications", *Oncotarget*, Vol. 8, No. 46, p. 81591, 2017.

15. Yu, Q., E. Rodriguez, R. Naccache, P. Forgione, G. Lamoureux, F. Sanz-

Rodriguez, D. Scheglmann and J. Capobianco, "Chemical Modification of Temoporfin-A Second Generation Photosensitizer Activated Using Upconverting Nanoparticles for Singlet Oxygen Generation", *Chemical Communications*, Vol. 50, No. 81, pp. 12150–12153, 2014.

16. Hu, S.-H., H.-M. Li, H. Yu, Y. Liu, C.-X. Liu, X.-B. Zuo, J. Lu, J.-J. Jiang, C.-X. Xi and B.-C. Huang, "Discovery of New Genetic Loci for Male Sexual Orientation in Han Population", *Cell Discovery*, Vol. 7, No. 1, pp. 1–14, 2021.

17. Huang, H., S. Mallidi, G. Obaid, B. Sears, S. Tangutoori and T. Hasan, "Advancing Photodynamic Therapy with Biochemically Tuned Liposomal Nanotechnologies", *Applications of Nanoscience in Photomedicine*, pp. 487–510, 2015.

18. Liu, H., Y. Liu, L. Wang, X. Ruan, F. Wang, D. Xu, J. Zhang, X. Jia and D. Liu, "Evaluation on Short-Term Therapeutic Effect of 2 Porphyrin Photosensitizer-Mediated Photodynamic Therapy for Esophageal Cancer", *Technology in Cancer Research & Treatment*, Vol. 18, p. 1533033819831989, 2019.

19. Wang, J., M. Zheng and Z. Xie, "Carrier-Free Core–Shell Nanodrugs for Synergistic Two-Photon Photodynamic Therapy of Cervical Cancer", *Journal of Colloid and Interface Science*, Vol. 535, pp. 84–91, 2019.

20. Hu, Y., J. F. Honek, B. C. Wilson and Q.-B. Lu, "Design, Synthesis and Photocytotoxicity of Upconversion Nanoparticles: Potential Applications for Near-Infrared Photodynamic and Photothermal Therapy", *Journal of Biophotonics*, Vol. 12, No. 11, p. e201900129, 2019.

21. Zhu, N., G. Xu, R. Wang, T. Zhu, J. Tan, X. Gu and C. Zhao, "Precise Imaging of Mitochondria in Cancer Cells by Real-Time Monitoring of Nitroreductase Activity with a Targetable and Activatable Fluorescent Probe", *Chemical Communications*, Vol. 56, No. 56, pp. 7761–7764, 2020.

22. Dougherty, T. J. and S. L. Marcus, "Photodynamic therapy", *European Journal of Cancer*, Vol. 28, No. 10, pp. 1734–1742, 1992.

23. Ferreira, J. T., J. Pina, C. A. Ribeiro, R. Fernandes, J. P. Tomé, M. S. Rodríguez-Morgade and T. Torres, "Highly Efficient Singlet Oxygen Generators Based on Ruthenium Phthalocyanines: Synthesis, Characterization and in Vitro Evaluation for Photodynamic Therapy", *Chemistry–A European Journal*, Vol. 26, No. 8, pp. 1789–1799, 2020.

24. Abrahamse, H. and M. R. Hamblin, "New Photosensitizers for Photodynamic Therapy", *Biochemical Journal*, Vol. 473, No. 4, pp. 347–364, 2016.

25. Kang, M., C. Zhou, S. Wu, B. Yu, Z. Zhang, N. Song, M. M. S. Lee, W. Xu, F.-J. Xu, D. Wang *et al.*, "Evaluation of Structure–Function Relationships of Aggregation-Induced Emission Luminogens for Simultaneous Dual Applications of Specific Discrimination and Efficient Photodynamic Killing of Gram-Positive Bacteria", *Journal of the American Chemical Society*, Vol. 141, No. 42, pp. 16781–16789, 2019.

26. Li, Q., Y. Li, T. Min, J. Gong, L. Du, D. L. Phillips, J. Liu, J. W. Lam, H. H. Sung, I. D. Williams *et al.*, "Time-Dependent Photodynamic Therapy for Multiple Targets: A Highly Efficient AIE-Active Photosensitizer for Selective Bacterial Elimination and Cancer Cell Ablation", *Angewandte Chemie International Edition*, Vol. 132, No. 24, pp. 9557–9564, 2020.

27. Chen, H., J. Tian, W. He and Z. Guo, "H2O2-Activatable and O2-Evolving Nanoparticles for Highly Efficient and Selective Photodynamic Therapy against Hypoxic Tumor Cells", *Journal of the American Chemical Society*, Vol. 137, No. 4, pp. 1539–1547, 2015.

28. Xia, B., B. Wang, J. Shi, Y. Zhang, Q. Zhang, Z. Chen and J. Li, "Photothermal and Biodegradable Polyaniline/Porous Silicon Hybrid Nanocomposites as Drug

Carriers for Combined Chemo-Photothermal Therapy of Cancer", *Acta Biomaterialia*, Vol. 51, pp. 197–208, 2017.

29. Askes, S. H., G. U. Reddy, R. Wyrwa, S. Bonnet and A. Schiller, "Red Light-Triggered CO Release from Mn2 (CO) 10 Using Triplet Sensitization in Polymer Nonwoven Fabrics", *Journal of the American Chemical Society*, Vol. 139, No. 43, pp. 15292–15295, 2017.

30. Francés-Monerris, A., I. Tuñón and A. Monari, "Hypoxia-Selective Dissociation Mechanism of a Nitroimidazole Nucleoside in a DNA Environment", *The Journal of Physical Chemistry Letters*, Vol. 10, No. 21, pp. 6750–6754, 2019.

31. García-Díaz, M., D. Sanchez-Garcia, J. Soriano, M. L. Sagristà, M. Mora, Á. Villanueva, J. C. Stockert, M. Cañete and S. Nonell, "Temocene: The Porphycene Analogue of Temoporfin (Foscan®)", *MedChemComm*, Vol. 2, No. 7, pp. 616–619, 2011.

32. Koca, B., E. Hamuryudan, S. Catak, A. Erdogmus, A. Monari and V. Aviyente, "Exploring The Photophysics of Polyfluorinated Phthalocyanine Derivatives as Potential Theranostic Agents", *The Journal of Physical Chemistry C*, Vol. 123, No. 40, pp. 24417–24425, 2019.

33. Li, Y., Y. Yu, L. Kang and Y. Lu, "Effects of Chlorin e6-Mediated Photodynamic Therapy on Human Colon Cancer SW480 Cells", *International Journal of Clinical and Experimental Medicine*, Vol. 7, No. 12, p. 4867, 2014.

34. Gattuso, H., A. Monari and M. Marazzi, "Photophysics of Chlorin e6: from One-and Two-Photon Absorption to Fluorescence and Phosphorescence", *RSC Advances*, Vol. 7, No. 18, pp. 10992–10999, 2017.

35. Kachynski, A., A. Pliss, A. Kuzmin, T. Ohulchanskyy, A. Baev, J. Qu and P. Prasad, "Photodynamic Therapy by in Situ Nonlinear Photon Conversion",

Nature Photonics, Vol. 8, No. 6, pp. 455–461, 2014.

36. Marazzi, M., H. Gattuso, A. Giussani, H. Zhang, M. Navarrete-Miguel, C. Chipot, W. Cai, D. Roca-Sanjuan, F. Dehez and A. Monari, "Induced Night Vision by Singlet-Oxygen-Mediated Activation of Rhodopsin", *The Journal of Physical Chemistry Letters*, Vol. 10, No. 22, pp. 7133–7140, 2019.

37. Zhou, Z., J. Liu, J. Huang, T. W. Rees, Y. Wang, H. Wang, X. Li, H. Chao and P. J. Stang, "A Self-Assembled Ru–Pt Metallacage as a Lysosome-Targeting Photosensitizer for 2-Photon Photodynamic Therapy", *Proceedings of the National Academy of Sciences*, Vol. 116, No. 41, pp. 20296–20302, 2019.

38. Chen, J., N. Mak, C. Yow, M. Fung, L. Chiu, W. Leung and N. Cheung, "The Binding Characteristics and Intracellular Localization of Temoporfin (mTHPC) in Myeloid Leukemia Cells: Phototoxicity and Mitochondrial Damage", *Photochemistry and Photobiology*, Vol. 72, No. 4, pp. 541–547, 2000.

39. Senge, M. O. and J. C. Brandt, "Temoporfin (Foscan®, 5, 10, 15, 20-Tetra (M-Hydroxyphenyl) Chlorin)—a Second-Generation Photosensitizer", *Photochemistry and Photobiology*, Vol. 87, No. 6, pp. 1240–1296, 2011.

40. Zimmermann, A., M. Ritsch-Marte and H. Kostron, "mTHPC-Mediated Photodynamic Diagnosis of Malignant Brain Tumors", *Photochemistry and Photobiology*, Vol. 74, No. 4, pp. 611–616, 2001.

41. De Vetta, M., O. Baig, D. Steen, J. J. Nogueira and L. González, "Assessing Configurational Sampling in the Quantum Mechanics/Molecular Mechanics Calculation of Temoporfin Absorption Spectrum and Triplet Density of States", *Molecules*, Vol. 23, No. 11, p. 2932, 2018.

42. De Vetta, M., O. Baig, D. Steen, J. J. Nogueira and L. González, "Assessing Configurational Sampling in the Quantum Mechanics/Molecular Mechanics

Calculation of Temoporfin Absorption Spectrum and Triplet Density of States", *Molecules*, Vol. 23, No. 11, p. 2932, 2018.

43. Zhao, Y., Z. Zhang, Z. Lu, H. Wang and Y. Tang, "Enhanced Energy Transfer in a Donor–Acceptor Photosensitizer Triggers Efficient Photodynamic Therapy", *ACS Applied Materials & Interfaces*, Vol. 11, No. 42, pp. 38467–38474, 2019.

44. Knoll, J. D. and C. Turro, "Control and Utilization of Ruthenium and Rhodium Metal complex Excited states for Photoactivated Cancer Therapy", *Coordination Chemistry Reviews*, Vol. 282, pp. 110–126, 2015.

45. Alves, S. R., I. R. Calori and A. C. Tedesco, "Photosensitizer-Based Metal-Organic Frameworks for Highly Effective Photodynamic Therapy", *Materials Science and Engineering: C*, Vol. 131, p. 112514, 2021.

46. Bächle, F., N. Siemens and T. Ziegler, "Glycoconjugated Phthalocyanines as Photosensitizers for PDT–Overcoming Aggregation in Solution", *European Journal of Organic Chemistry*, Vol. 2019, No. 42, pp. 7089–7116, 2019.

47. He, X., B. Situ, M. Gao, S. Guan, B. He, X. Ge, S. Li, M. Tao, H. Zou, B. Z. Tang *et al.*, "Stereotactic Photodynamic Therapy Using a Two-Photon AIE Photosensitizer", *Small*, Vol. 15, No. 50, p. 1905080, 2019.

48. Marazzi, M., H. Gattuso, A. Monari and X. Assfeld, "Steady-State Linear and Non-Linear Optical Spectroscopy of Organic Chromophores and Bio-Macromolecules", *Frontiers in Chemistry*, Vol. 6, p. 86, 2018.

49. Yakavets, I., H.-P. Lassalle, D. Scheglmann, A. Wiehe, V. Zorin and L. Bezdetnaya, "Temoporfin-in-Cyclodextrin-in-Liposome - A New Approach for Anticancer Drug Delivery: The Optimization of Composition", *Nanomaterials*, Vol. 8, No. 10, p. 847, 2018.

50. Yakavets, I., M. Millard, L. Lamy, A. Francois, D. Scheglmann, A. Wiehe, H.-P.

Lassalle, V. Zorin and L. Bezdetnaya, "Matryoshka-Type Liposomes Offer the Improved Delivery of Temoporfin to Tumor Spheroids", *Cancers*, Vol. 11, No. 9, p. 1366, 2019.

51. Yakavets, I., H.-P. Lassalle, I. Yankovsky, F. Ingrosso, A. Monari, L. Bezdetnaya and V. Zorin, "Evaluation of Temoporfin Affinity to β-cyclodextrins Assuming Self-Aggregation", *Journal of Photochemistry and Photobiology A: Chemistry*, Vol. 367, pp. 13–21, 2018.

52. Yakavets, I., I. Yankovsky, L. Bezdetnaya and V. Zorin, "Soret Band Shape Indicates mTHPC Distribution between β-cyclodextrins and Serum Proteins", *Dyes and Pigments*, Vol. 137, pp. 299–306, 2017.

53. Reshetov, V., D. Kachatkou, T. Shmigol, V. Zorin, M.-A. D'Hallewin, F. Guillemin and L. Bezdetnaya, "Redistribution of meta-tetra (hydroxyphenyl) chlorin (m-THPC) from Conventional and PEGylated Liposomes to Biological Substrates", *Photochemical Photobiological Sciences*, Vol. 10, No. 6, pp. 911–919, 2011.

54. Yankovsky, I., E. Bastien, I. Yakavets, I. Khludeyev, H.-P. Lassalle, S. Grafe, L. Bezdetnaya and V. Zorin, "Inclusion Complexation with β-cyclodextrin Derivatives Alters Photodynamic Activity and Biodistribution of meta-tetra (hydroxyphenyl) chlorin", *European Journal of Pharmaceutical Sciences*, Vol. 91, pp. 172–182, 2016.

55. Yakavets, I., I. Yankovsky, M. Millard, L. Lamy, H.-P. Lassalle, A. Wiehe, V. Zorin and L. Bezdetnaya, "The Alteration of Temoporfin Distribution in Multicellular Tumor Spheroids by β-cyclodextrins", *International Journal of Pharmaceutics*, Vol. 529, No. 1-2, pp. 568–575, 2017.

56. Cerezo, J., F. J. Avila Ferrer, G. Prampolini and F. Santoro, "Modeling Solvent Broadening on the Vibronic Spectra of a Series of Coumarin Dyes. From

Implicit to Explicit Solvent Models", *Journal of Chemical Theory and Computation*, Vol. 11, No. 12, pp. 5810–5825, 2015.

57. Barone, V., I. Cacelli, N. De Mitri, D. Licari, S. Monti and G. Prampolini, "J oyce and U lysses: Integrated and User-Friendly Tools for the Parameterization of Intramolecular Force Fields from Quantum Mechanical Data", *Physical Chemistry Chemical Physics*, Vol. 15, No. 11, pp. 3736–3751, 2013.

58. Prampolini, G., F. Ingrosso, A. Segalina, S. Caramori, P. Foggi and M. Pastore, "Dynamical and Environmental Effects on the Optical Properties of an Heteroleptic Ru (II)–Polypyridine Complex: A Multilevel Approach Combining Accurate Ground and Excited State QM-Derived Force Fields, MD and TD-DFT", *Journal of Chemical Theory and Computation*, Vol. 15, No. 1, pp. 529–545, 2018.

59. Aslanoglu, B., I. Yakavets, V. Zorin, H.-P. Lassalle, F. Ingrosso, A. Monari and S. Catak, "Optical Properties of Photodynamic Therapy Drugs in Different Environments: The Paradigmatic Case of Temoporfin", *Physical Chemistry Chemical Physics*, Vol. 22, No. 29, pp. 16956–16964, 2020.

60. Grimme, S., "Accurate Description of van der Waals Complexes by Density Functional Theory Including Empirical Corrections", *Journal of Computational Chemistry*, Vol. 25, No. 12, pp. 1463–1473, 2004.

61. Chai, J.-D. and M. Head-Gordon, "Long-Range Corrected Hybrid Density Functionals with Damped Atom–Atom Dispersion Corrections", *Physical Chemistry Chemical Physics*, Vol. 10, No. 44, pp. 6615–6620, 2008.

62. Slater, J. C., "Atomic Shielding Constants", *Physical Review*, Vol. 36, pp. 57–64, Jul 1930.

63. Boys, S. F., "Electronic Wave Functions-I. A General Method of Calculation for The Stationary States of Any Molecular System", *Proceedings of the Royal Society*

of London. Series A. Mathematical and Physical Sciences, Vol. 200, No. 1063, pp. 542–554, 1950.

64. Krishnan, R., J. S. Binkley, R. Seeger and J. A. Pople, "Self [U+2010] Consistent Molecular Orbital Methods. XX. A Basis Set for Correlated Wave Functions", *The Journal of Chemical Physics*, Vol. 72, No. 1, pp. 650–654, 1980.

65. "Ab Initio Study of Solvated Molecules: A New Implementation of The Polarizable Continuum Model", *Chemical Physics Letters*, Vol. 255, No. 4, pp. 327–335, 1996.

66. McFarland, S. A., A. Mandel, R. Dumoulin-White and G. Gasser, "Metal-Based Photosensitizers for Photodynamic Therapy: The Future of multimodal Oncology?", *Current Opinion in Chemical Biology*, Vol. 56, pp. 23–27, 2020.

67. Seritan, S., C. Bannwarth, B. S. Fales, E. G. Hohenstein, C. M. Isborn, S. I. Kokkila-Schumacher, X. Li, F. Liu, N. Luehr, J. W. Snyder Jr *et al.*, "TeraChem: A Graphical Processing Unit-Accelerated Electronic Structure Package for Large-Scale Ab Initio Molecular Dynamics", *Wiley Interdisciplinary Reviews: Computational Molecular Science*, Vol. 11, No. 2, p. e1494, 2021.

68. Isborn, C. M., A. W. Gotz, M. A. Clark, R. C. Walker and T. J. Martínez, "Electronic Absorption Spectra from MM and Ab Initio QM/MM Molecular Dynamics: Environmental Effects on the Absorption Spectrum of Photoactive Yellow Protein", *Journal of Chemical Theory and Computation*, Vol. 8, No. 12, pp. 5092–5106, 2012.

69. Phillips, J. C., R. Braun, W. Wang, J. Gumbart, E. Tajkhorshid, E. Villa, C. Chipot, R. D. Skeel, L. Kale and K. Schulten, "Scalable Molecular Dynamics with NAMD", *Journal of computational chemistry*, Vol. 26, No. 16, pp. 1781–1802, 2005.

70. Feller, S. E., Y. Zhang, R. W. Pastor and B. R. Brooks, "Constant Pressure Molecular Dynamics Simulation: The Langevin Piston Method", *The Journal of Chemical Physics*, Vol. 103, No. 11, pp. 4613–4621, 1995.

71. Davidchack, R. L., R. Handel and M. Tretyakov, "Langevin Thermostat for Rigid Body Dynamics", *The Journal of Chemical Physics*, Vol. 130, No. 23, p. 234101, 2009.

72. Hoover, W. G., "Constant-Pressure Equations of Motion", *Physical Review A*, Vol. 34, No. 3, p. 2499, 1986.

73. Essmann, U., L. Perera, M. L. Berkowitz, T. Darden, H. Lee and L. G. Pedersen, "A Smooth Particle Mesh Ewald Method", *The Journal of Chemical Physics*, Vol. 103, No. 19, pp. 8577–8593, 1995.

74. Wang, J., R. M. Wolf, J. W. Caldwell, P. A. Kollman and D. A. Case, "Development and Testing of a General Amber Force Field", *Journal of Computational Chemistry*, Vol. 25, No. 9, pp. 1157–1174, 2004.

75. Ivanova, N. and A. Ivanova, "Testing the Limits of Model Membrane Simulations—Bilayer Composition and Pressure Scaling", *Journal of Computational Chemistry*, Vol. 39, No. 8, pp. 387–396, 2018.

76. Pluhackova, K., S. A. Kirsch, J. Han, L. Sun, Z. Jiang, T. Unruh and R. A. Bo¨ckmann, "A Critical Comparison of Biomembrane Force Fields: Structure and Dynamics of Model DMPC, POPC, and POPE Bilayers", *The Journal of Physical Chemistry B*, Vol. 120, No. 16, pp. 3888–3903, 2016.

77. Marrink, S. J., V. Corradi, P. C. Souza, H. I. Ingolfsson, D. P. Tieleman and M. S. Sansom, "Computational Modeling of Realistic Cell Membranes", *Chemical Reviews*, Vol. 119, No. 9, pp. 6184–6226, 2019.

78. Mark, P. and L. Nilsson, "Structure and Dynamics of the TIP3P, SPC, and SPC/E

Water Models at 298 K", *The Journal of Physical Chemistry A*, Vol. 105, No. 43, pp. 9954–9960, 2001.

79. Humphrey, W., A. Dalke and K. Schulten, "VMD: Visual Molecular Dynamics", *Journal of Molecular Graphics*, Vol. 14, No. 1, pp. 33–38, 1996.

80. Contreras-García, J., E. R. Johnson, S. Keinan, R. Chaudret, J.-P. Piquemal, D. N. Beratan and W. Yang, "NCIPLOT: A Program for Plotting Noncovalent Interaction Regions", *Journal of Chemical Theory and Computation*, Vol. 7, No. 3, pp. 625–632, 2011.

81. Yakavets, I., H.-P. Lassalle, I. Yankovsky, F. Ingrosso, A. Monari, L. Bezdetnaya and V. Zorin, "Evaluation of Temoporfin Affinity to β-cyclodextrins Assuming Self-Aggregation", *Journal of Photochemistry and Photobiology A: Chemistry*, Vol. 367, pp. 13–21, 2018.

82. Koca, B., E. Hamuryudan, S. Catak, A. Erdogmus, A. Monari and V. Aviyente, "Exploring the Photophysics of Polyfluorinated Phthalocyanine Derivatives as Potential Theranostic Agents", *The Journal of Physical Chemistry C*, Vol. 123, No. 40, pp. 24417–24425, 2019.

83. Etienne, T., T. Very, E. A. Perpète, A. Monari and X. Assfeld, "A QM/MM Study of the Absorption Spectrum of Harmane in Water Solution and Interacting with DNA: the Crucial Role of Dynamic Effects", *The Journal of Physical Chemistry B*, Vol. 117, No. 17, pp. 4973–4980, 2013.

84. Gattuso, H., M. Marazzi, F. Dehez and A. Monari, "Deciphering the Photosensitization Mechanisms of Hypericin Towards Biological Membranes", *Physical Chemistry Chemical Physics*, Vol. 19, No. 34, pp. 23187–23193, 2017.

85. Segalina, A., X. Assfeld, A. Monari and M. Pastore, "Computational Modeling of Exciton Localization in Self-Assembled Perylene Helices: Effects of Thermal

Motion and Aggregate Size", *The Journal of Physical Chemistry C*, Vol. 123, No. 11, pp. 6427–6437, 2019.

86. Li, Y., Y. Yu, L. Kang and Y. Lu, "Effects of Chlorin e6-Mediated Photodynamic Therapy on Human Colon Cancer SW480 Cells", *International Journal of Clinical and Experimental medicine*, Vol. 7, No. 12, p. 4867, 2014.

87. Sengul, O., E. B. Boydas, M. Pastore, W. Sharmouk, P. C. Gros, S. Catak and A. Monari, "Probing Optical Properties of Thiophene Derivatives for Two-Photon Absorption", *Theoretical Chemistry Accounts*, Vol. 136, No. 6, pp. 1–9, 2017.

88. Marazzi, M., H. Gattuso, A. Monari and X. Assfeld, "Steady-State Linear and Non-Linear Optical Spectroscopy of Organic Chromophores and Bio-Macromolecules", *Frontiers in Chemistry*, Vol. 6, p. 86, 2018.

89. Neto, A. J. and R. M. Cordeiro, "Molecular Simulations of the Effects of Phospholipid and Cholesterol Peroxidation on Lipid Membrane Properties", *Biochimica et Biophysica Acta (BBA)-Biomembranes*, Vol. 1858, No. 9, pp. 2191–2198, 2016.

90. Tasso, T. T., J. C. Schlothauer, H. C. Junqueira, T. A. Matias, K. Araki, E. Liandra-Salvador, F. C. Antonio, P. Homem-de Mello and M. S. Baptista, "Photobleaching Efficiency Parallels the Enhancement of Membrane Damage for Porphyrazine Photosensitizers", *Journal of the American Chemical Society*, Vol. 141, No. 39, pp. 15547–15556, 2019.

91. Bacellar, I. O., M. C. Oliveira, L. S. Dantas, E. B. Costa, H. C. Junqueira, W. K. Martins, A. M. Durantini, G. Cosa, P. Di Mascio, M. Wainwright *et al.*, "Photosensitized Membrane Permeabilization Requires Contact-Dependent Reactions between Photosensitizer and Lipids", *Journal of the American Chemical Society*, Vol. 140, No. 30, pp. 9606–9615, 2018.

92. Van Bay, M., N. K. Hien, P. T. D. Tran, N. T. K. Tuyen, D. T. Y. Oanh, P. C.

Nam and D. T. Quang, "TD-DFT Benchmark for UV-Vis Spectra of Coumarin Derivatives", *Vietnam Journal of Chemistry*, Vol. 59, No. 2, pp. 203–210, 2021.

93. Zeng, Q., Z. Li, Y. Dong, A. Qin, Y. Hong, L. Ji, Z. Zhu, C. K. Jim, G. Yu, Q. Li *et al.*, "Fluorescence Enhancements of Benzene-Cored Luminophors by Restricted Intramolecular Rotations: AIE and AIEE Effects", *Chemical Communications*, Vol. 1, pp. 70–72, 2007.

94. Yang, H., X. Zhou, T. Hui, Y. Han, X. Jiang and J. Yan, "Methyl-Restricted Rotor Rotation on the Stator Produces High-Efficiency Fluorescence Emission: A New Strategy to Achieve Aggregation-Induced Emission", *RSC Advances*, Vol. 9, No. 21, pp. 12078–12084, 2019.

95. Etienne, T., L. Chbibi, C. Michaux, E. A. Perpete, X. Assfeld and A. Monari, "All-Organic Chromophores for Dye-Sensitized Solar Cells: A Theoretical Study on Aggregation", *Dyes and Pigments*, Vol. 101, pp. 203–211, 2014.

96. Kasha, M., "Energy Transfer Mechanisms and the Molecular Exciton Model for Molecular Aggregates", *Radiation Research*, Vol. 20, No. 1, pp. 55–70, 1963.

97. Hestand, N. J. and F. C. Spano, "Molecular Aggregate Photophysics beyond the Kasha Model: Novel Sesign Principles for Organic Materials", *Accounts of Chemical Research*, Vol. 50, No. 2, pp. 341–350, 2017.

98. Santoro, F., R. Improta, A. Lami, J. Bloino and V. Barone, "Effective Method to Compute Franck-Condon Integrals for Optical Spectra of Large Molecules in Solution", *The Journal of Chemical Physics*, Vol. 126, No. 8, p. 084509, 2007.

99. Improta, R., V. Barone and F. Santoro, "Ab Initio Calculations of Absorption Spectra of Large Molecules in Solution: Coumarin C153", *Angewandte Chemie International Edition*, Vol. 46, No. 3, pp. 405–408, 2007.

100. Cerezo, J., D. Aranda, F. J. Avila Ferrer, G. Prampolini and F. Santoro,

"Adiabatic-Molecular Dynamics Generalized Vertical Hessian Approach: A Mixed Quantum Classical Method to Compute Electronic Spectra of Flexible Molecules in the Condensed Phase", *Journal of Chemical Theory and Computation*, Vol. 16, No. 2, pp. 1215–1231, 2019.

101. Infield, D. T., A. Rasouli, G. D. Galles, C. Chipot, E. Tajkhorshid and C. A. Ahern, "Cation-π Interactions and Their Functional Roles in Membrane Proteins", *Journal of Molecular Biology*, Vol. 433, No. 17, p. 167035, 2021.

102. Varsano, D., S. Caprasecca and E. Coccia, "Theoretical Description of Protein Field Effects on Electronic Excitations of Biological Chromophores", *Journal of Physics: Condensed Matter*, Vol. 29, No. 1, p. 013002, 2016.

APPENDIX A: ARTICLES

A.1. Optical Properties of Photodynamic Therapy Drugs in Different Environments: The Paradigmatic Case of Temoporfin

A full-text version of the first article regarding part I is given in this section.

ROYAL SOCIETY OF CHEMISTRY

PCCP

PAPER

View Article Online
View Journal | View Issue

Open Access Article. Published on 16 July 2020. Downloaded on 6/3/2021 12:10:52 PM.
This article is licensed under a Creative Commons Attribution 3.0 Unported Licence.

Check for updates

Cite this: *Phys. Chem. Chem. Phys.*, 2020, 22, 16956

Optical properties of photodynamic therapy drugs in different environments: the paradigmatic case of temoporfin†

Busenur Aslanoglu,[a] Ilya Yakavets,[bcd] Vladimir Zorin,[be] Henri-Pierre Lassalle,[cd] Francesca Ingrosso,[f] Antonio Monari *[f] and Saron Catak *[a]

Received 16th April 2020,
Accepted 24th June 2020

DOI: 10.1039/d0cp02055a

rsc.li/pccp

Computational tools have been used to study the photophysical and photochemical features of photosensitizers in photodynamic therapy (PDT) – a minimally invasive, less aggressive alternative for cancer treatment. PDT is mainly based on the activation of molecular oxygen through the action of a photoexcited sensitizer (photosensitizer). Temoporfin, widely known as mTHPC, is a second-generation photosensitizer, which produces the cytotoxic singlet oxygen when irradiated with visible light and hence destroys tumor cells. However, the bioavailability of the mostly hydrophobic photosensitizer, and hence its incorporation into cells, is fundamental to achieve the desired effect on malignant tissues *via* PDT. In this study, we focus on the optical properties of the temoporfin chromophore in different environments – *in vacuo*, in solution, encapsulated in drug delivery agents, namely cyclodextrin, and interacting with a lipid bilayer.

Introduction

The exploitation of light as a therapeutic agent for the treatment of diverse and problematic diseases has gained large popularity in the last few decades,[1] paving the way to the definition of novel and less invasive, yet efficient, therapeutic strategies.[2] This has most notably involved the treatment of bacterial and viral diseases,[3,4] as well as more debilitating conditions such as some type of cancers.[5–7] However, the use of light for therapeutic purposes may be traced back to Ancient Greece, where exposure to sunlight, termed heliotherapy, was commonly used to treat a variety of conditions, including muscular weakness and skin diseases.[7,8] The importance of such practices is also reflected in the fact that the god Apollon was associated with both medicine and the sun.

Today the therapeutic use of light has evolved considerably, particularly owing to the milestone discovery and application of photodynamic therapy (PDT).[9,10] In this context, a drug that is inert in the dark is administered to a patient, either topically or systemically, and the region in which the lesion is localized is then irradiated, usually with visible or infrared light.[11] The absorption of light by the drug – the photosensitizer – triggers photophysical pathways leading to the disruption of biological macromolecules (nucleic acids, proteins, or lipid membranes) and, consequently, to cell death, and ultimately to the eradication of the lesion.[12]

Although photophysical or photochemical pathways subsequent to light absorption may be diverse, two main families of events can be underlined: type I reactions involve either hydrogen abstraction or electron transfer from the excited photosensitizer (PS) to a substrate molecule to produce free radicals or radical ions.[13] Type II reactions transfer energy to molecular oxygen to produce singlet oxygen ($^1O_2$).[14] In particular, type II pathways usually proceed through intersystem crossing (ISC) populating the photosensitizer's triplet state manifold allowing the activation of the molecular oxygen from its triplet ($^3O_2$) to singlet ($^1O_2$) state.[15] Subsequently, the action of $^1O_2$ will induce the oxidative stress responsible for cell death.[16] PDT has proven efficient in the treatment of a variety of diseases, including psoriasis[17] as well as certain types of cancer,[18] such as esophageal[19] and cervical,[20] greatly limiting the side-effect of conventional therapy due to the spatial-selectivity of irradiation.[21,22]

[a] *Bogazici University, Department of Chemistry, Bebek 34342, Istanbul, Turkey. E-mail: saron.catak@boun.edu.tr*
[b] *Laboratory of Biophysics and Biotechnology, Belarussian State University, 220030, Minsk, Belarus*
[c] *Université de Lorraine and CNRS, CRAN, UMR 7039, F-54000, Nancy, France*
[d] *Université de Lorraine, Institut de Cancérologie de Lorraine, F-54000, Nancy, France*
[e] *International Sakharov Environmental Institute, 220030, Minsk, Belarus*
[f] *Université de Lorraine and CNRS, LPCT, UMR 7019, F-54000, Nancy, France. E-mail: antonio.monari@univ-lorraine.fr*

† Electronic supplementary information (ESI) available: Dihedral distributions, RMSD plots, free rotation plot, experimental UV/VIS spectral data for mTHPC in water, TM-b-CD and POPC, Cartesian coordinates for mTHPC. See DOI: 10.1039/d0cp02055a

93 C. M. Isborn, N. Luehr, I. S. Ufimtsev and T. J. Martínez, *J. Chem. Theory Comput.*, 2011, 7, 1814–1823.
94 R. Bonnett, P. Charlesworth, B. D. Djelal, S. Foley,

This journal is © the Owner Societies 2020

Figure A.1. Optical Properties of Photodynamic Therapy Drugs in Different Environments: The Paradigmatic Case of Temoporfin

Open Access Article. Published on 16 July 2020. Downloaded on 6/3/2021 12:10:52 PM.
This article is licensed under a Creative Commons Attribution 3.0 Unported Licence.

There are several requirements that should be met by PDT agents to increase their efficiency and guarantee their therapeutic effects.[23] These include: facile ISC, high quantum yield for the production of $^1O_2$,[24] absorption in the red or infrared portion of the electromagnetic spectrum to cover the therapeutic window for which penetration into tissues is maximal,[25] as well as enhanced selectivity towards bacterial[26] or cancer cells.[27] However, the need for oxygen activation in PDT may present an obstacle for the treatment of hypoxic solid tumors.[28] Hence, the exploitation of different photochemical pathways, such as photodissociation, have been proposed under the general name of light-assisted chemotherapy (LAC).[29–32] The displacement of the absorption spectrum towards the red is also pursued *via* different chemical strategies, including the use of organometallic complexes,[33,34] or enlarging the conjugation pattern of the sensitizers.[35] More recently, the exploitation of non-linear optics, two-photon absorption (TPA)[36–39] in particular, has been suggested.

Although various agents have been proposed for PDT and LAC, nowadays, the quasi-totality of clinically approved agents are based on porphyrins,[40,41] phthalocyanines,[42] or chlorins.[43–46] These classes of molecules display red-shifted absorption, which may be further modulated by the inclusion of metal in the coordination sphere,[42,47,48] relatively good ISC quantum yields as well as versatile and economic synthetic viability. On the other hand, their efficacy is somewhat limited by solubility issues[49] and by aggregation phenomena[50] that severely limit their bioavailability and lead to excited-state deactivation channels hampering the triplet population.

One of the most efficient PDT drugs on the market nowadays, yet still plagued by aggregations,[51] is the so-called temoporfin (5,10,15,20-tetrakis(3-hydroxyphenyl)chlorin – mTHPC, Fig. 1a and b). Marketed in the EU under the brand name Foscan,[52] mTHPC is a synthetic tetrapyrrole, a partially hydrogenated porphyrin derivative, known as chlorin (Fig. 1a). Temoporfin is a second-generation photosensitizer, which has higher skin penetration, deeper light penetration, and lower biotoxicity, and moreover, it requires shorter treatment time as well as a lower light dosage to achieve the desired PDT response compared with other clinically approved photosensitizers, such as hematoporphyrin derivatives and photofirin.[52] Indeed, mTHPC possesses appropriate photophysical properties: excitation to the first excited singlet state by red light (630–680 nm),[53] and efficient ISC to a longer-lived excited triplet state, which has recently been rationalized by molecular modeling.[54] The latter triplet state may produce cytotoxic species by either a type I or type II reaction typical of photosensitizer agents used in photodynamic therapy.[55]

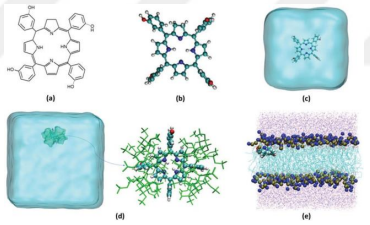

Fig. 1 Representative structures of mTHPC used in this study: (a) 2D representation (b) 3D representation, (c) mTHPC in water, (d) mTHPC:TM-b-cyclodextrin complex in water, and (e) mTHPC interacting with a lipid bilayer surrounded by water.

As mentioned, the most serious drawback of mTHPC, and many other organic sensitizers, is their hydrophobic nature, which severely limits their transportation in the bloodstream and causes aggregation-induced quenching (ACQ) in biological environments,[56] hence resulting in weak emissions and inadequate generation of reactive oxygen species (ROS).[57] To overcome the mTHPC aggregation issue, specific drug delivery strategies are currently being pursued,[58] in particular, the use of molecular hosts based on beta-cyclodextrin (b-CD) has been proposed.[59,60] The incorporation of mTHPC into beta-cyclodextrin[61] (Fig. 1d) and its release in model lipid membranes[62,63] (Fig. 1e) and cells[64,65] have been experimentally assessed by monitoring its fluorescence quenching. Most notably, the encapsulation of mTHPC in trimethyl-b-cyclodextrin (TM-b-CD) also produces a strong enhancement of the fluorescence quantum yield that is almost totally quenched in solution, hence allowing for the possibility to efficiently follow drug delivery by optical spectroscopy.

A clear rationalization of the different aspects of PDT at the atomistic and electronic levels represents a challenge, since it requires multiscale modelling that is able to deal with both the treatment of excited states and the sampling of complex environments. In this respect, the development of PDT drug delivery systems represents a most paradigmatic case, since it requires the proper exploration of the conformational space of complex systems in complex environments, and at the same time, the need to provide a balanced description of physical and chemical phenomena taking place in both the ground and excited state manifolds.[66] In particular, the complex systems involved in drug delivery and their interactions with biological structures requires the use of dynamic simulations using force field-based descriptions, also due to the key temporal spans that need to be covered. However, the sensitivity of excited state properties to even the slightest structural modifications also requires careful parameterization of the force fields.[67–69]

In this study, we report the optical and photophysical properties of mTHPC employing molecular simulations in different environments: (a) *in vacuo*, (b) in solution, (c) in solution encapsulated within TM-b-cyclodextrin (mTHPC:TM-b-CD complex), and (d) in interaction with a lipid bilayer mimicking a biological membrane. Herein, we provide a clear rationalization of the optical properties of the most relevant PDT drug; the coupling between its critical structural parameters, the degrees of freedom of different molecular environments, such as drug delivery systems or cellular compartments, and the effects of heterogeneous environments on its photophysical properties.

Optical Properties of Photodynamic Therapy Drugs in Different Environments: The Paradigmatic Case of Temoporfin. Article 1. (cont.)

Open Access Article. Published on 16 July 2020. Downloaded on 6/3/2021 12:10:52 PM.
This article is licensed under a Creative Commons Attribution 3.0 Unported Licence.

The interactions of mTHPC with a model biological membrane will also help rationalize its efficiency as a PDT agent.

Methodology

Computational approach

Structural and optical properties of mTHPC were investigated with quantum mechanical/molecular dynamics (QM/MD) and classical MD simulations in different environments, namely in vacuum, in water, in complex with the TM-b-CD, and in contact with a model lipid bilayer composed of 1-palmitolyl-2-oleyl-*sn*-*glycero*-3-phosphocholine (POPC).

Classical molecular dynamics and force field parameterization

Classical MD simulations were conducted using the NAMD program package.[70] All simulations were carried out in the constant pressure and temperature ensemble (*NPT*)[71] at 1 atm and 300.0 K, a time step of 2.0 fs was used to integrate Newton's equations of motion. A production run of 100 ns was performed after equilibration and thermalization, temperature and pressure were controlled by Langevin thermostat[72] and Nosé–Hoover Langevin barostat,[73,74] respectively. Periodic boundary conditions (PBC) were used and the Particle Mesh Ewald (PME) expansion[75] was applied to calculate long-range electrostatics contributions with a 9 Å cutoff distance.

The force field for mTHPC was parametrized with Generalized Amber Force Field (GAFF),[76] while point charges were obtained by fitting to the restricted electrostatic potential (RESP) using the Antechamber program.[77] GLYCAM06[78] was used for the parametrization of TM-b-CD. mTHPC was solvated by a cubic water box of 50.0 × 50.0 × 50.0 Å^3, while the mTHPC:TM-b-CD complex was prepared considering a 1 : 2 stoichiometry (Fig. 1d) as suggested by previous work[61] and solvated in a water box (90.0 × 85.0 × 85.0 Å^3).

Lipid14 General Amber Force Field[79] was used to represent the POPC unit, while the lipid bilayer was set up with the CHARMM-GUI Membrane interface.[80,81] 100 POPC units were used in each membrane leaflet, the bilayer was fully hydrated with 37 551 water molecules and was neutralized by 104 K^+ and Cl^- ions, the total simulation box size is 81.0 × 81.0 × 138.0 Å^3. POPC is the most widely used lipid model to simulate biological membranes. Indeed, a single lipid membrane model is an oversimplification of a biological environment, since the structural properties of the membrane may also be affected by the presence of other fatty acids or cholesterol. However, the use of a single lipid, greatly reduces the degrees of freedom, while still providing a realistic amphiphilic model that discriminates between the polar head and the lipid core region.[82–84]

The TIP3P water model[85] was consistently used in all the simulated systems. MD simulations were visualized and analyzed *via* the VMD code;[86] the most relevant non-covalent interactions (NCI) throughout the MD trajectories were analyzed and depicted with NCIPlot code.[87] The study of the gradient of the electronic density clearly differentiates NCIs in terms of steric clashes, dispersion, and hydrogen bonding.

Quantum mechanics molecular dynamics

Hybrid quantum mechanics/molecular mechanics molecular dynamic simulations[88] (QM/MM MD) were performed to sample the ground state conformational space by the Terachem/Amber[89] and NAMD/Terachem interface.[90] mTHPC was included in the QM partition and described by the B3LYP[91] density functional and 6-31G basis set. Water and TM-b-CD were treated at the MM level of theory, with the force field parameterization previously described. For details of the QM/MM simulations, see ESI,† (Table S1).

Electronic structure calculations

Single point energy calculations and geometry optimizations were performed using the Gaussian 09 program package[92] with Density Functional Theory (DFT) at B3LYP[91] and 6-31G(d) basis set level of theory. The potential energy surface scan to parameterize the mTHPC force field and the conformational analysis were performed with the same level of theory, the energies along the scan have also been estimated using the second order Moller–Plesset perturbation theory (MP2).

To simulate the absorption spectra, vertical electronic excitations from the ground state were obtained *via* time-dependent DFT[93] (TD-DFT). The choice of the exchange–correlation functional and basis set were further justified by a benchmark on the calculation of the vertical excitation energies from the ground state equilibrium geometry reported in ESI.† While the influence of the basis set on the excitation energies appears to be negligible, the functional has a more pronounced effect. More specifically, oB97X-D and M06-2X provide the correct separation of the Q_x and Q_y bands, in the red wavelengths domain, while B3LYP only yields an unresolved broad band. Hence, oB97XD/6-31G(d) clearly represents the best compromise between computational cost and accuracy, and was chosen to further take into account the dynamical and vibrational effects. To this end, all UV-vis absorption spectra were generated from the convolution of vertical excitations from 100 snapshots randomly extracted from the MD trajectories. The convolution of the vertical excitation energies and oscillator strengths was performed using Gaussian functions of full width at half-length (FWHL) of 0.15 eV.

Experimental procedures

Materials

The photosensitizer, mTHPC, was kindly provided by Biolitec research GmbH (Jena, Germany) with purity >99%. TM-b-CD (purity >98%, M.W. 1430 Da) was purchased from AraChem (Tilburg, the Netherlands). b-CDs in the powder were weighed and then dissolved in Dulbecco's phosphate-buffered saline (DPBS) (pH 7.4) at 4 °C at the final concentration of 10 mM using molar weight provided by the supplier. mTHPC stock solution (2 mM) was prepared in absolute ethanol (99.6%) and was kept at 4 °C in the dark. mTHPC concentration in the solution was estimated by means of a spectrophotometric method using molar extinction coefficient of 30 000 M^{-1} cm^{-1} at 650 nm in ethanol.[94]

Inclusion complexes between b-CDs and mTHPC were formed using the co-precipitation method.[95] Briefly, the stock ethanol

93 C. M. Isborn, N. Luehr, I. S. Ufimtsev and T. J. Martínez, *J. Chem. Theory Comput.*, 2011, 7, 1814–1823.

This journal is © the Owner Societies 2020

Figure A.1.Optical Properties of Photodynamic Therapy Drugs in Different Environments: The Paradigmatic Case of Temoporfin. Article 1. (cont.)

View Article Online

Open Access Article. Published on 16 July 2020. Downloaded on 6/3/2021 12:10:52 PM.
This article is licensed under a Creative Commons Attribution 3.0 Unported Licence.

solution of mTHPC (2 mM) was added to TM-b-CDs dissolved in DPBS (pH 7.4) at 4 ıC and 1 mM. The final content of ethanol in the mTHPC/b-CD solutions did not exceed 0.5%. The solution was thoroughly mixed for 15 min under magnetic stirring.

Spectroscopic measurements

Absorption spectra were recorded using a Lambda 35 spectrophotometer (PerkinElmer, USA) using 1 cm optical path quartz cuvettes. All spectroscopic measurements were carried out in triplicate at room temperature (23–25 ıC). The optical density of all samples did not exceed 0.3 a.u.

Results and discussion

In the following section, we report the structural and optical properties of mTHPC in molecular environments of increasing complexity. Using molecular simulations, the interaction of temoporfin with water, TM-b-CD and a lipid bilayer is modelled, and subsequently compared with the corresponding experimental data, when available. For this purpose, different levels of theory are employed, the evolution of critical structural parameters along with photophysical properties are assessed, and the effect of the molecular environment is comparatively discussed.

mTHPC is composed of four functionalized phenols that adorn the core chlorin ring. The phenol rings constitute one of the leading factors potentially inducing specific intermolecular interactions with the environment, such as hydrogen bonds, while the chlorin core will be the most crucial unit dictating the optical properties of the chromophore. In addition, the inclusion of mTHPC in the TM-b-CD complex will also determine the orientation of the peripheral substituents and will, in turn, modify their flexibility. Hence, a proper parameterization of the force field to catch all these subtle phenomena, and in particular, the rotational flexibility of the phenol substituents with respect to the chlorin core is crucial.

Dihedral angles defining the rotation of the peripheral phenolic groups of mTHPC are depicted in Fig. 2. While full rotations are not expected to take place due to clashes between the phenyl hydrogens and the porphyrin core; phenolic moieties are expected to span a much wider range in gas phase and in solution. However, this may change considerably in the cyclodextrin complex due to much larger steric hindrance. As previously demonstrated, the mTHPC:TM-b-CD complex has a 1 : 2 stoichiometry[61] (Fig. 1d) and is held together by dispersion interactions between the two TM-b-CD that globally shelter the hydrophobic mTHPC from the water environment.

A gas-phase QM scan of Temoporfin's peripheral dihedral angle, performed both at DFT and MP2 level of theory (Fig. S2–S3, ESI†), confirms a large degree of freedom of the phenolic group as seen by the nearly flat potential energy curve in the 60–120ı region. The sharp increase in the potential energy around 0ı and 180ı is due to steric repulsion with the core and is indicative of the emergence of two distinct conformers. Hence, to properly represent this situation a free rotation of the phenol ring was implemented in the classical force field for mTHPC by setting the force constant to zero, the results for the distribution of the dihedral angles in the different environments obtained with the classical force field match remarkably the ones of the QM or QM/MM MD. Note that the mTHPC FF was parametrized to better represent the PS in confined environments, hence, it is somewhat expected that its performance will be less adequate *in vacuo* and in solution where the rotational flexibility is larger.

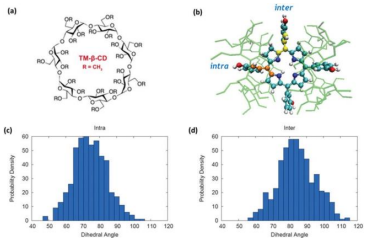

Fig. 2 (a) 2D structure of TM-b-CD (b) temoporfin-cyclodextrin complex (mTHPC : TM-b-CD) showing 1 : 2 stoichiometric ratio and two non-identical dihedrals; intra (in orange) and inter (in yellow). Dihedral angles defining the rotation of the peripheral phenolic groups of mTHPC (c) intra (C19–C20–C21–C22) dihedral angle distribution histogram (d) inter (C4–C5–C39–C40) dihedral angle distribution histogram from QM/MM MD calculations.

In addition to the globally reduced flexibility, two different situations occur in the temoporfin-cyclodextrin complex (mTHPC:TM-b-CD complex), potentially presenting differences in steric hindrance due to the specific complexation pattern. As seen in Fig. 2b, two of the phenolic groups of Temoporfin are located inside the cyclodextrin pockets (intra), while the other two reside in the hydrophobic region between the two cyclodextrins (inter). In addition to the reduced mobility evidenced by the sharper distribution reported in Fig. 2, as compared to the water case (Fig. S10–S12, ESI†), subtle differences also emerge between the intra and inter distributions, where the intra-phenol appears to experience a slightly more impeded rotation than the inter (Fig. 2c and d). This is probably due to the highly constrained interior of the cyclodextrin core that is explored by the intra-phenol moeity. The reduced mobility of the phenol rings in the macromolecular complex as opposed to the gas phase or solution may also offer an additional reason for the enhancement of fluorescence observed in the host complex. The free rotation of the peripheral moieties would offer a further non-radiative decay pathway that will lead to the deactivation of the excited state. Indeed, the restricted intramolecular rotation has been recognized as a cause of the fluorescence enhancement in different organic luminophores.[96,97] As it is the case for diverse fluorophores,[98–100] the aggregation of chromophores, and hence the formation of dark excitonic states, could also be considered as a supplementary phenomenon leading to fluorescence quenching in solution.

Figure A.1.Optical Properties of Photodynamic Therapy Drugs in Different Environments: The Paradigmatic Case of Temoporfin. Article 1. (cont.)

View Article Online

Open Access Article. Published on 16 July 2020. Downloaded on 6/3/2021 12:10:52 PM.
This article is licensed under a Creative Commons Attribution 3.0 Unported Licence.

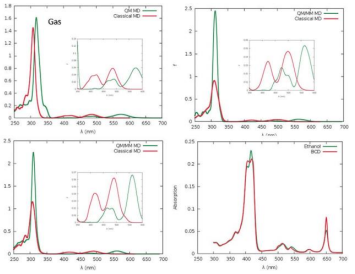

Fig. 3 Experimental and computational absorption spectrum in different environments (a) mTHPC in vacuum, (b) mTHPC in water, (c) mTHPC:TM-b-CD in water, the ground state conformational space has been sampled either with classical MD (red spectrum) or QM/MM MD (green curve), and (d) experimental data.

The experimental absorption spectra of mTHPC are reported in Fig. 3, and unsurprisingly present all the features of chlorin-based chromophores. In particular, the absorption bands in the 500–680 nm region, corresponding to the Q-bands, as well as the more intense Soret bands in the blue region. It is evident from the analysis of the QM based MD simulation of mTHPC in the gas phase (Fig. S6, ESI†), as well as the QM/MM MD simulation of mTHPC in solution (Fig. S10, ESI†) that two low-energy large-amplitude degrees of freedom dominate the conformational space: the out-of-plane deformation of the conjugated ring system and the rotation of the peripheral phenolic units. These degrees of freedom are critical in describing the global vibration of the drug and may have an influence on the observed optical properties. The out-of-plane normal modes may be responsible for the red-shift of the absorption spectra with respect to vertical transitions calculated from the ground state geometry only (Fig. 3 and ESI†) due to the significant destabilization of the ground state rather than the excited state, as is common for similar p-conjugated systems.[42,44,101–103] Although the influence of the rotation of the peripheral substituents on the absorption spectral maxima is expected to be marginal, it may, nonetheless, induce a broadening of the absorption and emission bands, and more notably, may have a key role in inducing thermal quenching of the luminescence. While the possibility to take into account the out-of-plane deformation effects *via* a reasonable sampling of the conformational space is well established and has been thoroughly demonstrated in similar systems,[36,42,66,101] the effects of the peripheral dihedral rotations require much deeper attention, due to their strong non-harmonic behaviour. In addition, the effect of the molecular surrounding, and in particular of the embedding in confined environments, such as cyclodextrin, should be properly taken into account.

In Fig. 3, we also report the comparison between the absorption spectra calculated as the convolution of vertical transitions from a series of snapshots obtained by sampling mTHPC's conformational space with either a QM/MM approach, in which the whole chromophore is treated quantum mechanically, or a MM approach, in which the dynamics of the chromophore is described by a force field. The agreement between the different levels of the theory is good, confirming the validity of the chosen approach, the only difference being the slightly more red shifted Q-band obtained with the QM/MM. Interestingly, the Q-band region also appears more sensitive to the specific chemical environment, in particular for the absorption spectrum of the mTHPC:TM-b-CD. Indeed, in this case, the inversion of the intensity between the Q_x and Q_y Soret bands observed experimentally, constituting one of the spectroscopic signatures of complex formation, is clearly identified and nicely reproduced by the full classic and the hybrid sampling protocol.

The reasonable agreement between the calculated spectroscopic properties also constitutes a further validation of the novel force field, with an obvious improvement over the parametrization used in our previous work.[61] Note that experimental results have been conducted in ethanol instead of water,[104,105] because of the global low solubility of the sensitizers. In the simulations, we decided to use water as a solvent to mimic the most biologically relevant solvent. Moreover, the protic nature of ethanol solvent should lead to a similar solvatochromic effect as water.

Having established the robustness and precision of our force field parameterization that has been validated by means of different levels of theory and proven to reproduce both the structural parameters and the optical properties of mTHPC in different environments, we move to examine the interaction, between the chromophore and a lipid bilayer. Indeed, the mode of action as a PDT drug should involve the disruption of the cell membrane induced by the activated $^1O_2$ following the absorption of light. The results of the MD simulation are reported in Fig. 4 in the form of the density profile along the membrane axis for the main functional group and pictorially using a representative snapshot. At the beginning of the simulation the photosensitizer is placed in bulk water and unsurprisingly, due to its hydrophobic nature, mTHPC develops favorable interactions with the lipid membrane with a persistence time exceeding hundreds of ns.

In the obtained most stable configuration, mTHPC is positioned around the polar head regions, and more precisely, at the interface between the phosphate and the fatty acid hydrophobic core. Indeed, mTHPC is more exposed to the lipid environment than to the water bulk. This behaviour is not totally unexpected and can be traced back to the concomitant presence of a hydrophobic core and phenol groups that may develop specific non-covalent interactions with the polar head regions. However, the position of mTHPC is most favorable for PDT purposes. Indeed, while O_2 will permeate the membrane due to its hydrophobic nature as also revealed by MD simulations,[106] it will also have a non-negligible concentration in the region occupied by the photosensitizer. In addition, our density profile also shows that mTHPC partially overlaps with the position of the lipid carbon–carbon double bond. This fact indicates that $^1O_2$ will be produced in close proximity to its

Figure A.1.Optical Properties of Photodynamic Therapy Drugs in Different Environments: The Paradigmatic Case of Temoporfin. Article 1. (cont.)

View Article Online

Open Access Article. Published on 16 July 2020. Downloaded on 6/3/2021 12:10:52 PM.
This article is licensed under a Creative Commons Attribution 3.0 Unported Licence.

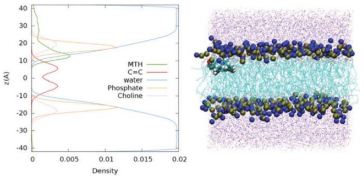

Fig. 4 Density Profile along the membrane axis and a representative snapshot showing mTHPC embedded in a POPC lipid bilayer.

reactive target, hence minimizing the quenching probability. It has also been reported that photosensitizers, also porphyrin-based, may exert photopermeabilization of the lipid membrane *via* an alternative contact dependent mechanism, that involves electron abstraction from solvent or lipids.[107,108] Although further studies, including the modelling of additional membrane components, such as cholesterol, should be needed to confirm this scenario, our density profile, and the partial overlap identified, claims in favour of the possibility of this photophysical route, concerning the chromophore positioning and the key geometrical factors.

To better characterize the factors influencing the stability of the persistent aggregate evidenced in the MD trajectory, we performed a detailed analysis of the specific interactions taking place between mTHPC and the lipid constituents. As reported in Fig. 5, in addition to dispersion interactions typical of hydrophobic compounds, the formation of specific interactions mainly involving hydrogen-bonding between the phenol groups and the negatively charged phosphates, contributes to locking the chromophore at the interface region.

This interaction, as well as its persistence, is confirmed by the structure of the radial distribution function presented in Fig. 5a, for the involved phenolic hydroxyl and the phosphate oxygen groups. The sharp peak at around 1.6 Å is very indicative of a typical and persistent hydrogen bond. The same conclusions can be drawn from the NCI plots for some representative snapshots. The features of a hydrogen bond formation, represented by the concentrated green circle around the phosphate and phenol group, are indeed clearly evident in the zoom of Fig. 5a. Although the hydrogen bonding pattern was somewhat expected, other non-covalent interactions are also pertinent, namely, the cation–p interactions between the aromatic mTHPC core and the positively charged choline in the lipid head groups are clearly evidenced both by the radial distribution function and by the NCI plot (Fig. 5b). In addition, as evidenced in the ESI,† the more structured and viscous environment offered by the lipid bilayer induces a partial rigidification of mTHPC, and hence a more impeded rotation around the phenol rings. However, this situation is much weaker than the one observed in the case of the cyclodextrin complex, the enhancement of fluorescence observed when mTHPC is in the presence of biological membranes should, hence, be mainly ascribed to the absence of p-stacking (aggregation).[62,63,109]

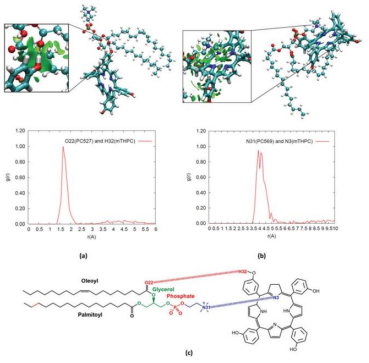

Fig. 5 Radial distribution functions and NCI plots for (a) hydrogen bonding (b) cation–p interactions between mTHPC and the lipid bilayer. (c) 2D structure of POPC lipid and mTHPC, highlighting the interacting atoms.

The absorption spectrum calculated in the POPC interface is also reported in Fig. 6 and shows that most of the characteristic spectral features are maintained. Indeed, both the Q and the Soret bands are clearly distinguishable, and interestingly, in contrast with what was observed in the case of the mTHPC:TM-b-CD complex, no inversion between the Q_x and Q_y band is observed. However, the energy differences between the two bands are underestimated by our computational approach, as compared to experiment. This difference could mostly be ascribed to the neglect of purely quantum vibronic coupling through the explicit calculation of Franck–Condon parameters.[110,111] However, such an approach, despite some interesting recent developments, is still far from being standardized.[112]

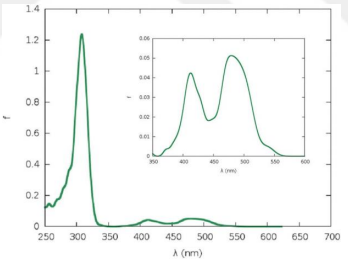

Fig. 6 Absorption spectra of mTHPC embedded in POPC lipid bilayer.

93 C. M. Isborn, N. Luehr, I. S. Ufimtsev and T. J. Martínez, *J. Chem. Theory Comput.*, 2011, 7, 1814–1823.

Figure A.1.Optical Properties of Photodynamic Therapy Drugs in Different Environments: The Paradigmatic Case of Temoporfin. Article 1. (cont.)

View Article Online

Open Access Article. Published on 16 July 2020. Downloaded on 6/3/2021 12:10:52 PM.
This article is licensed under a Creative Commons Attribution 3.0 Unported Licence.

Conclusions

In this contribution, we report the detailed analysis of the structural and optical properties of a known photosensitizer, mTHPC, clinically used for PDT purposes in different complex environments, including a cyclodextrin-based encapsulating drug delivery agent, and a model lipid bilayer. Our results show that the confined environment of the cyclodextrin induces a strong reduction of the mobility of the peripheral phenol rings. Furthermore, clear differences in the mobility degree appear for intra and inter substituents. The strong reduction of the phenyl ring rotation is also correlating well with the observed enhancement of the fluorescence quantum yield upon encapsulation. Our results have also highlighted the formation of persistent aggregates between mTHPC and lipid membranes, with the sensitizer residing preferentially in the interface between the polar heads and the lipid core. This situation is favoured by interactions, such as the formation of hydrogen bonds and cation–p interactions with the polar heads that counterbalances the hydrophobic dispersion interactions developed with the lipid core. Interestingly, the position of the sensitizer represents one of the most ideal ones for PDT purposes, since it encompasses both the area of maximum oxygen concentration and a partial overlap with the position of the oxidizable lipid double-bond. In addition, the optical properties have been determined, including the sampling of the conformational space of the ground state, highlighting a rather marginal, but non-innocent, effect of the environment and the necessity to carefully parameterize the crucial force-field parameters.

In the future, we plan to pursue the study of mTHPC interactions with cyclodextrins and lipid membranes in a twofold perspective. From the one side, the release from the encapsulating complex and the subsequent insertion in the lipid membrane will be studied by using enhanced sampling techniques. In addition, the intersystem crossing, and hence the population of the triplet state manifold, for mTHPC in different environments will be studied including the possibility to perform QM/MM based non-adiabatic dynamics to quantitatively assess the quantum yield and timescales of the first event of the photosensitization chain.

Conflicts of interest

There are no conflicts to declare.

Acknowledgements

Calculations were partially performed at the TUBITAK ULAKBIM High Performance and Grid Computing Center (TRUBA resources), the LPCT (www.lpct.univ-lorraine.fr) local computing resources as well as the computational resources at CCBG (www.ccbg.boun.edu.tr) funded by the Bogazici University Research Fund (BAP-SUP Project No. 8245). The authors thank biolitec research GmbH (Jena, Germany) for providing with mTHPC.

References

1 Y. Wang, J. Zhao, Z. Chen, F. Zhang, Q. Wang, W. Guo, K. Wang, H. Lin and F. Qu, *Biomaterials*, 2019, 217, 119282.
2 N. Philbrick, *Smithsonian*, 2016, 2795–2838.
3 A. Azizi, P. Shohrati, M. Goudarzi, S. Lawaf and A. Rahimi, *Photodiagn. Photodyn. Ther.*, 2019, 27, 203–209.
4 J. Shen, Q. Liang, G. Su, Y. Zhang, Z. Wang, C. Baudouin and A. Labbé, *Transl. Vis. Sci. Technol.*, 2019, 8, 1–10.
5 L. Zhang, Z. Ji, J. Zhang and S. Yang, *Photodiagn. Photodyn. Ther.*, 2019, 28, 159–165.
6 M. Hamblin, *Photochem. Photobiol.*, 2020, 96, 506–516.
7 P. Jarrett and R. Scragg, *Photochem. Photobiol. Sci.*, 2017, 16, 283–290.
8 T. Karppinen, L. Ylianttila, H. Kautiainen, T. Reunala and E. Snellman, *Acta Derm. – Venereol.*, 2015, 95, 579–582.
9 J. Zhang, C. Jiang, J. P. Figueirô Longo, R. B. Azevedo, H. Zhang and L. A. Muehlmann, *Acta Pharm. Sin. B*, 2018, 8, 137–146.
10 R. L. Yanovsky, D. W. Bartenstein, G. S. Rogers, S. J. Isakoff and S. T. Chen, *Photodermatol., Photoimmunol. Photomed.*, 2019, 35, 295–303.
11 P. Majumdar, R. Nomula and J. Zhao, *J. Mater. Chem. C*, 2014, 2, 5982–5997.
12 E. Buytaert, M. Dewaele and P. Agostinis, *Biochim. Biophys. Acta, Rev. Cancer*, 2007, 1776, 86–107.
13 Y.-Y. Wang, Y.-C. Liu, H. Sun and D.-S. Guo, *Coord. Chem. Rev.*, 2019, 395, 46–62.
14 Z. Tan, J. Zhang, L. Lin and B. Li, in *Optics in Health Care and Biomedical Optics VII*, ed. Q. Luo, X. Li, Y. Gu and Y. Tang, 2016, vol. 10024, p. 100241C.
15 J. Kou, D. Dou and L. Yang, *Oncotarget*, 2017, 8, 81591–81603.
16 Q. Yu, E. M. Rodriguez, R. Naccache, P. Forgione, G. Lamoureux, F. Sanz-Rodriguez, D. Scheglmann and J. A. Capobianco, *Chem. Commun.*, 2014, 50, 12150–12153.
17 F. Yi, X. Zheng, F. Fang, J. Zhang, B. Zhou and X. Chen, *Exp. Dermatol.*, 2019, 0–3.
18 H.-C. Huang, S. Mallidi, G. Obaid, B. Sears, S. Tangutoori and T. Hasan, *Applications of Nanoscience in Photomedicine*, Elsevier, 2015, pp. 487–510.
19 H. Liu, Y. Liu, L. Wang, X. Ruan, F. Wang, D. Xu, J. Zhang, X. Jia and D. Liu, *Technol. Cancer Res. Treat.*, 2019, 18, 1–6.
20 J. Wang, M. Zheng and Z. Xie, *J. Colloid Interface Sci.*, 2019, 535, 84–91.
21 Y. Hu, J. F. Honek, B. C. Wilson and Q. B. Lu, *J. Biophotonics*, 2019, 12, 1–11.
22 Y. Ni, H. Zhang, C. Chai, B. Peng, A. Zhao, J. Zhang, L. Li, C. Zhang, B. Ma, H. Bai, K. L. Lim and W. Huang, *Adv. Healthcare Mater.*, 2019, 8, 1–9.
23 T. J. Dougherty and S. L. Marcus, *Eur. J. Cancer*, 1992, 28, 1734–1742.
24 J. T. Ferreira, J. Pina, C. A. F. Ribeiro, R. Fernandes, J. P. C. Tomé, M. S. Rodríguez-Morgade and T. Torres, *Chem. – Eur. J.*, 2020, 26, 1789–1799.
25 H. Abrahamse and M. R. Hamblin, *Biochem. J.*, 2016, 473, 347–364.

Figure A.1.Optical Properties of Photodynamic Therapy Drugs in Different Environments: The Paradigmatic Case of Temoporfin. Article 1. (cont.)

View Article Online

Open Access Article. Published on 16 July 2020. Downloaded on 6/3/2021 12:10:52 PM.
This article is licensed under a Creative Commons Attribution 3.0 Unported Licence.

1 M. Kang, C. Zhou, S. Wu, B. Yu, Z. Zhang, N. Song, M. M. S. Lee, W. Xu, F.-J. Xu, D. Wang, L. Wang and B. Z. Tang, *J. Am. Chem. Soc.*, 2019, 141, 16781–16789.
2 Q. Li, Y. Li, T. Min, J. Gong, L. Du, D. L. Phillips, J. Liu, J. W. Y. Lam, H. H. Y. Sung, I. D. Williams, R. T. K. Kwok, C. L. Ho, K. Li, J. Wang and B. Z. Tang, *Angew. Chem., Int. Ed.*, 2020, 59, 9470–9477.
3 H. Chen, J. Tian, W. He and Z. Guo, *J. Am. Chem. Soc.*, 2015, 137, 1539–1547.
4 B. Xia, B. Wang, J. Shi, Y. Zhang, Q. Zhang, Z. Chen and J. Li, *Acta Biomater.*, 2017, 51, 197–208.
5 S. Bonnet, B. Limburg, J. D. Meeldijk, R. J. M. K. Gebbink and J. A. Killian, *J. Am. Chem. Soc.*, 2011, 133, 252–261.
6 S. H. C. Askes, G. U. Reddy, R. Wyrwa, S. Bonnet and A. Schiller, *J. Am. Chem. Soc.*, 2017, 139, 15292–15295.
7 A. Francés-Monerris, I. Tuñón and A. Monari, *J. Phys. Chem. Lett.*, 2019, 10, 6750–6754.
8 Y. Zhao, Z. Zhang, Z. Lu, H. Wang and Y. Tang, *ACS Appl. Mater. Interfaces*, 2019, 11, 38467–38474.
9 J. D. Knoll and C. Turro, *Coord. Chem. Rev.*, 2015, 282–283, 110–126.
10 L. Li, B. Bae, T. H. Tran, K. H. Yoon, K. Na and K. M. Huh, *Carbohydr. Polym.*, 2011, 86, 708–715.
11 O. Sengul, E. B. Boydas, M. Pastore, W. Sharmouk, P. C. Gros, S. Catak and A. Monari, *Theor. Chem. Acc.*, 2017, 136, 67.
12 J. D. Bhawalkar, N. D. Kumar, C. F. Zhao and P. N. Prasad, *J. Clin. Laser Med. Surg.*, 1997, 15, 201–204.
13 Y. Shen, A. J. Shuhendler, D. Ye, J. J. Xu and H. Y. Chen, *Chem. Soc. Rev.*, 2016, 45, 6725–6741.
14 F. Bolze, S. Jenni, A. Sour and V. Heitz, *Chem. Commun.*, 2017, 53, 12857–12877.
15 J. W. Hofman, M. G. Carstens, F. V. Zeeland, C. Helwig, F. M. Flesch, W. E. Hennink and C. F. V. Nostrum, *Pharm. Res.*, 2008, 25, 2065–2073.
16 M. García-Díaz, D. Sánchez-García, J. Soriano, M. L. Sagristà, M. Mora, Á. Villanueva, J. C. Stockert, M. Cañete and S. Nonell, *MedChemComm*, 2011, 2, 616–619.
17 B. Koca, E. Hamuryudan, S. Catak, A. Erdogmus, A. Monari and V. Aviyente, *J. Phys. Chem. C*, 2019, 123, 24417–24425.
18 Y. Li, Y. Yu, L. Kang and Y. Lu, *Int. J. Clin. Exp. Med.*, 2014, 7, 4867–4876.
19 H. Gattuso, A. Monari and M. Marazzi, *RSC Adv.*, 2017, 7, 10992–10999.
20 A. V. Kachynski, A. Pliss, A. N. Kuzmin, T. Y. Ohulchanskyy, A. Baev, J. Qu and P. N. Prasad, *Nat. Photonics*, 2014, 8, 1–7.
21 M. Marazzi, H. Gattuso, A. Giussani, H. Zhang, M. Navarrete-Miguel, C. Chipot, W. Cai, D. Roca-Sanjuán, F. Dehez and A. Monari, *J. Phys. Chem. Lett.*, 2019, 10, 7133–7140.
22 Z. Zhou, J. Liu, J. Huang, T. W. Rees, Y. Wang, H. Wang, X. Li, H. Chao and P. J. Stang, *Proc. Natl. Acad. Sci. U. S. A.*, 2019, 116, 20296–20302.
23 Z. Zhang, W. Sang, L. Xie and Y. Dai, *Coord. Chem. Rev.*, 2019, 399, 213022.
24 X. Lu, W. Zhu, T. Chen, Q. Peng, C. Yu and M. Yang, *Chem. Phys. Lett.*, 2019, 735, 136737.
25 Z. Liu, Y. Xue, M. Wu, G. Yang, M. Lan and W. Zhang, *Biomacromolecules*, 2019, 20, 4563–4573, DOI: acs.biomac.9b01368.
26 J. Y. Chen, N. K. Mak, C. M. N. Yow, M. C. Fung, L. C. Chiu, W. N. Leung and N. H. Cheung, *Photochem. Photobiol.*, 2000, 72, 541.
27 M. O. Senge and J. C. Brandt, *Photochem. Photobiol.*, 2011, 87, 1240–1296.
28 W. M. Sharman, C. M. Allen and J. E. V. Lier, *Drug Discovery Today*, 1999, 4, 507–517.
29 M. De Vetta, O. Baig, D. Steen, J. J. Nogueira and L. González, *Molecules*, 2018, 23, 2932.
30 A. D. Quartarolo, D. Pérusse, F. Dumoulin, N. Russo and E. Sicilia, *J. Porphyrins Phthalocyanines*, 2013, 17, 980–988.
31 F. Bächle, N. Siemens and T. Ziegler, *Eur. J. Inorg. Chem.*, 2019, 7089–7116.
32 X. He, B. Situ, M. Gao, S. Guan, B. He, X. Ge, S. Li, M. Tao, H. Zou, B. Z. Tang and L. Zheng, *Small*, 2019, 1905080, 1–8.
33 I. Yakavets, M. Millard, V. Zorin, H. P. Lassalle and L. Bezdetnaya, *J. Controlled Release*, 2019, 304, 268–287.
34 I. Yakavets, H. P. Lassalle, D. Scheglmann, A. Wiehe, V. Zorin and L. Bezdetnaya, *Nanomaterials*, 2018, 8, 1–15.
35 I. Yakavets, M. Millard, L. Lamy, A. Francois, D. Scheglmann, A. Wiehe, H. P. Lassalle, V. Zorin and L. Bezdetnaya, *Cancers*, 2019, 11, 1–16.
36 I. Yakavets, H. P. Lassalle, I. Yankovsky, F. Ingrosso, A. Monari, L. Bezdetnaya and V. Zorin, *J. Photochem. Photobiol., A*, 2018, 367, 13–21.
37 I. Yakavets, I. Yankovsky, L. Bezdetnaya and V. Zorin, *Dyes Pigm.*, 2017, 137, 299–306.
38 V. Reshetov, D. Kachatkou, T. Shmigol, V. Zorin, M. A. D'Hallewin, F. Guillemin and L. Bezdetnaya, *Photochem. Photobiol. Sci.*, 2011, 10, 911–919.
39 I. Yankovsky, E. Bastien, I. Yakavets, I. Khludeyev, H. P. Lassalle, S. Gräfe, L. Bezdetnaya and V. Zorin, *Eur. J. Pharm. Sci.*, 2016, 91, 172–182.
40 I. Yakavets, I. Yankovsky, M. Millard, L. Lamy, H. P. Lassalle, A. Wiehe, V. Zorin and L. Bezdetnaya, *Int. J. Pharm.*, 2017, 529, 568–575.
41 X. Assfeld, A. Monari, M. Marazzi and H. Gattuso, *Front. Chem.*, 2018, 6, 86.
42 J. Cerezo, F. J. Avila Ferrer, G. Prampolini and F. Santoro, *J. Chem. Theory Comput.*, 2015, 11, 5810–5825.
43 V. Barone, I. Cacelli, N. De Mitri, D. Licari, S. Monti and G. Prampolini, *Phys. Chem. Chem. Phys.*, 2013, 15, 3736–3751.
44 G. Prampolini, F. Ingrosso, A. Segalina, S. Caramori, P. Foggi and M. Pastore, *J. Chem. Theory Comput.*, 2019, 15, 529–545.
45 J. C. Phillips, R. Braun, W. Wang, J. Gumbart, E. Tajkhorshid, E. Villa, C. Chipot, R. D. Skeel, L. Kalé and K. Schulten, *J. Comput. Chem.*, 2005, 26, 1781–1802.
46 S. E. Feller, Y. Zhang, R. W. Pastor and B. R. Brooks, *J. Chem. Phys.*, 1995, 103, 4613–4621.
47 R. L. Davidchack, R. Handel and M. V. Tretyakov, *J. Chem. Phys.*, 2009, 130, 234101.
48 W. G. Hoover, *Phys. Rev. A: At., Mol., Opt. Phys.*, 1986, 34, 2499–2500.

Figure A.1.Optical Properties of Photodynamic Therapy Drugs in Different Environments: The Paradigmatic Case of Temoporfin. Article 1. (cont.)

View Article Online

Open Access Article. Published on 16 July 2020. Downloaded on 6/3/2021 12:10:52 PM.
This article is licensed under a Creative Commons Attribution 3.0 Unported Licence.

1 P. Procacci, S. Marsili, A. Barducci, G. F. Signorini and R. Chelli, *J. Chem. Phys.*, 2006, 125, 164101.
2 U. Essmann, L. Perera, M. L. Berkowitz, T. Darden, H. Lee and L. G. Pedersen, *J. Chem. Phys.*, 1995, 103, 8577–8593.
3 J. Wang, R. M. Wolf, J. W. Caldwell, P. A. Kollman and D. A. Case, *J. Comput. Chem.*, 2004, 25, 1157–1174.
4 J. Wang, W. Wang, P. A. Kollman and D. A. Case, *J. Mol. Graphics Modell.*, 2006, 25, 247–260.
5 A. Uhe, S. Kozuch and S. Shaik, *J. Comput. Chem.*, 2010, 1–8.
6 C. J. Dickson, B. D. Madej, Å. A. Skjevik, R. M. Betz, K. Teigen, I. R. Gould and R. C. Walker, *J. Chem. Theory Comput.*, 2014, 10, 865–879.
7 E. L. Wu, X. Cheng, S. Jo, H. Rui, K. C. Song, E. M. Dávila-Contreras, Y. Qi, J. Lee, V. Monje-Galvan, R. M. Venable, J. B. Klauda and W. Im, *J. Comput. Chem.*, 2014, 35,1997–2004.
8 S. Jo, J. B. Lim, J. B. Klauda and W. Im, *Biophys. J.*, 2009, 97, 50–58.
9 N. Ivanova and A. Ivanova, *J. Comput. Chem.*, 2018, 39, 387–396.
10 K. Pluhackova, S. A. Kirsch, J. Han, L. Sun, Z. Jiang, T. Unruh and R. A. Böckmann, *J. Phys. Chem. B*, 2016, 120, 3888–3903.
11 S. J. Marrink, V. Corradi, P. C. T. Souza, H. I. Ingólfsson, D. P. Tieleman and M. S. P. Sansom, *Chem. Rev.*, 2019, 119, 6184–6226.
12 P. Marck and L. Nilsson, *J. Phys. Chem. A*, 2001, 105, 9954–9960.
13 W. Humphrey, A. Dalke and K. Schulten, *J. Mol. Graphics*, 1996, 14(33–38), 27–28.
14 J. Contreras-García, E. R. Johnson, S. Keinan, R. Chaudret, J. Piquemal, D. N. Beratan and W. Yang, *J. Chem. Theory Comput.*, 2011, 7, 625–632.
15 J. Sgrignani and A. Magistrato, *ACS Catal.*, 2015, 5, 3864–3875.
16 C. M. Isborn, A. W. Götz, M. A. Clark, R. C. Walker and T. J. Martínez, *J. Chem. Theory Comput.*, 2012, 8, 5092–5106.
17 M. C. R. Melo, R. C. Bernardi, T. Rudack, M. Scheurer, C. Riplinger, J. C. Phillips, J. D. C. Maia, G. B. Rocha, J. V. Ribeiro, J. E. Stone, F. Neese, K. Schulten and Z. Luthey-Schulten, *Nat. Methods*, 2018, 15, 351–354.
91 A. Becke, *J. Chem. Phys.*, 1993, 98, 5648–5652.
92 W. C. Frisch, M. J. Trucks, G. W. Schlegel, H. B. Scuseria, G. E. Robb, M. A. Cheeseman, J. R. Scalmani, G. Barone, V. Mennucci, B. Petersson, G. A. Nakatsuji, H. Caricato, M. Li, X. Hratchian, H. P. Izmaylov, A. F. Bloino, J. Zheng and G. Sonnenb, 2009.
93 C. M. Isborn, N. Luehr, I. S. Ufimtsev and T. J. Martínez, *J. Chem. Theory Comput.*, 2011, 7, 1814–1823.
94 R. Bonnett, P. Charlesworth, B. D. Djelal, S. Foley, D. J. Mcgarvey and T. G. Truscott, *In Vivo*, 1999, 325–328.
95 E. M. M. D. Valle, *Process Biochem.*, 2004, 39, 1033–1046.
96 Q. Zeng, Z. Li, Y. Dong, C. Di, A. Qin, Y. Hong, L. Ji, Z. Zhu, C. K. W. Jim, G. Yu, Q. Li, Z. Li, Y. Liu, J. Qin and B. Z. Tang, *Chem. Commun.*, 2007, 70–72.
97 H. Yang, X. Zhou, T. Hui, Y. Han, X. Jiang and J. Yan, *RSC Adv.*, 2019, 9, 12078–12084.
98 T. Etienne, L. Chbibi, C. Michaux, E. A. Perpète, X. Assfeld and A. Monari, *Dyes Pigm.*, 2014, 101, 203–211.
99 M. Kasha, *Radiat. Res.*, 1963, 20, 55.
100 N. J. Hestand and F. C. Spano, *Acc. Chem. Res.*, 2017, 50, 341–350.
101 T. Etienne, T. Very, E. A. Perpète, A. Monari and X. Assfeld, *J. Phys. Chem. B*, 2013, 117, 4973–4980.
102 H. Gattuso, M. Marazzi, F. Dehez and A. Monari, *Phys. Chem. Chem. Phys.*, 2017, 19, 23187–23193.
103 A. Segalina, X. Assfeld, A. Monari and M. Pastore, *J. Phys. Chem. C*, 2019, 123, 6427–6437.
104 M. Millard, I. Yakavetsa, M. Piffoux, A. Brun, F. Gazeau, J. M. Guigner, J. Jasniewski, H. P. Lassalle, C. Wilhelm and L. Bezdetnaya, *Drug Delivery*, 2018, 25, 1790–1801.
105 C. Lange, C. Lehmann, M. Mahler and P. J. Bednarski, *Comparison of cellular death pathways after mTHPC-mediated photodynamic therapy (PDT) in five human cancer cell lines*, 2019, vol. 11.
106 R. M. Cordeiro, *Biochim. Biophys. Acta, Biomembr.*, 2014, 1838, 438–444.
107 T. T. Tasso, J. C. Schlothauer, H. C. Junqueira, T. A. Matias, K. Araki, É. Liandra-Salvador, F. C. T. Antonio, P. Homem-De-Mello and M. S. Baptista, *J. Am. Chem. Soc.*, 2019, 141, 15547–15556.
108 I. O. L. Bacellar, M. C. Oliveira, L. S. Dantas, E. B. Costa, H. C. Junqueira, W. K. Martins, A. M. Durantini, G. Cosa, P. Di Mascio, M. Wainwright, R. Miotto, R. M. Cordeiro, S. Miyamoto and M. S. Baptista, *J. Am. Chem. Soc.*, 2018, 140, 9606–9615.
109 M. De Vetta, L. González and J. J. Nogueira, *ChemistryOpen*, 2018, 7, 475–483.
110 F. Santoro, R. Improta, A. Lami, J. Bloino and V. Barone, *J. Chem. Phys.*, 2007, 126, 084509.
111 R. Improta, V. Barone and F. Santoro, *Angew. Chem., Int. Ed.*, 2007, 46, 405–408.
112 J. Cerezo, D. Aranda, F. J. Avila Ferrer, G. Prampolini and F. Santoro, *J. Chem. Theory Comput.*, 2020, 16, 1215–1231.

Figure A.1.Optical Properties of Photodynamic Therapy Drugs in Different Environments: The Paradigmatic Case of Temoporfin. Article 1. (cont.)

APPENDIX B: Root-Mean-Square-Deviation Values of mTHPC from different environments

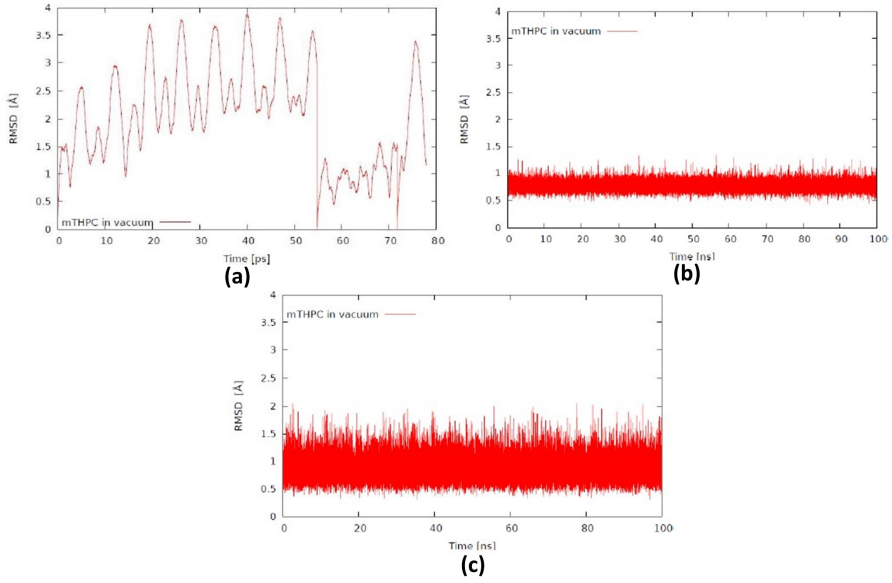

Figure B.1. mTHPC in vacuum calculation from (a) QM/MD (b) oldFF (c) newFF

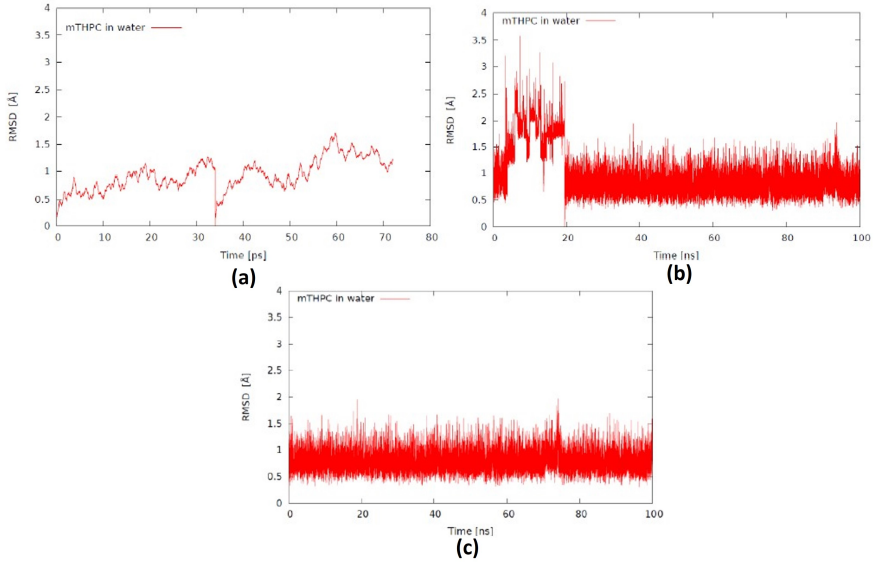

Figure B.2. mTHPC in water calculation from (a) QM/MD (b) oldFF (c) newFF

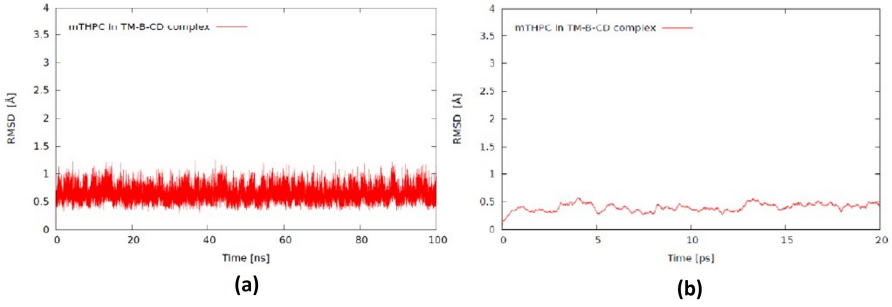

Figure B.3. mTHPC in TM-β-CD calculation from (a) newFF (b) QM/MD

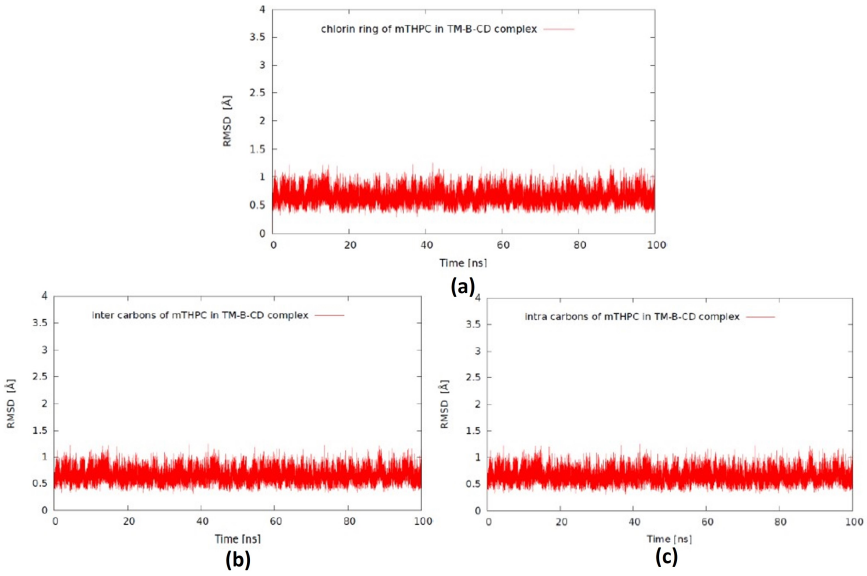

Figure B.4. mTHPC in TM-β-CD calculation from (a) newFF (b) carbon atoms of mTHPC at inter position (c) carbon atoms of mTHPC at inter position

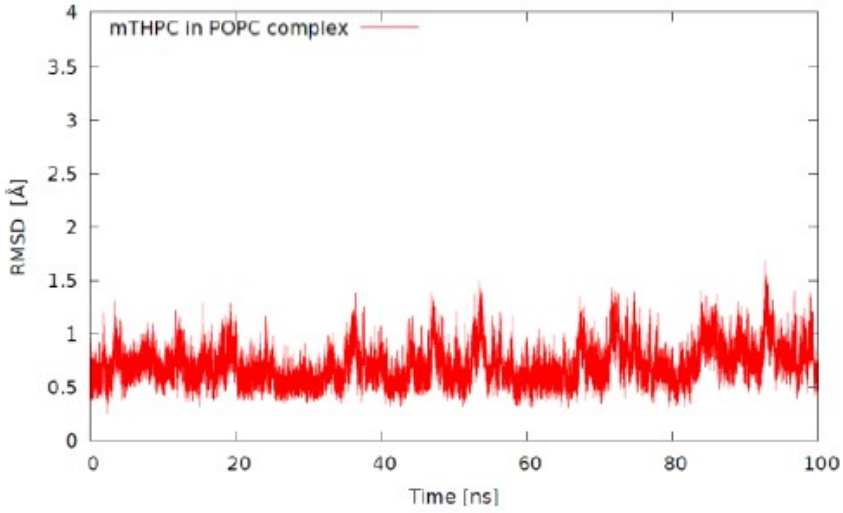

Figure B.5. mTHPC in POPC lipid bilayer from Classical MD calculation with newFF